Sequential bone marrow-cell delivery of VEGFA/S1P improves vascularization and limits adverse cardiac remodeling after myocardial infarction in mice

Magdalena M. Żak[1], Polyxeni Gkontra [1], Cristina Clemente [1], Mario Leonardo Squadrito[2], Alessia Ferrarini[3], Rubén A. Mota[4], Eduardo Oliver[5], Susana Rocha[1], Jaume Agüero[5,6], Jesús Vázquez[3,6], Michele De Palma[2], Borja Ibáñez[5,6], and Alicia G. Arroyo[1,7$]

[1]Vascular Pathophysiology Area, [3]Proteomics Unit, [4]Animal Facility, [5]Myocardial Pathology Area. Centro Nacional de Investigaciones Cardiovasculares (CNIC), Melchor Fernández Almagro 3, 28029 Madrid, Spain

[2]Ecole Polytechnique Federale de Lausanne (EPFL), ISREC-Swiss Institute for Experimental Cancer Research, SV 2527 (SV building), Station 19, CH-1015 Lausanne

[6]CIBER-CV, Madrid, Spain

[7]Present address: Centro de Investigaciones Biológicas (CIB-CSIC), Madrid, Spain

$Corresponding author
Alicia G. Arroyo
Vascular Pathophysiology Area
Centro Nacional de Investigaciones Cardiovasculares (CNIC)
Melchor Fernández Almagro 3
28021 Madrid
Spain
Phone 34 91 4531200
e-mail agarroyo@cnic.es

Running title: VEGFA/S1P cardiac angiotherapy

Keywords: VEGFA, S1P, gene-cell angiotherapy, myocardial infarction, oxygen diffusion, cardiac remodeling

Abstract: 200 words

5 Figures, 1 Supp Table and 5 Supp Figures

Abstract

Microvascular dysfunction and resulting tissue hypoxia is a major contributor to the pathogenesis and evolution of cardiovascular diseases (CVD). Diverse gene and cell therapies have been proposed to preserve the microvasculature or boost angiogenesis in CVD with moderate benefit. In this study, we tested *in vivo* the impact of sequential delivery by bone marrow cells of the pro-angiogenic factors vascular endothelial growth factor (VEGFA) and sphingosine-1-phosphate (S1P) in a myocardial infarction model. For that we transduced mouse bone marrow cells with lentiviral vectors coding for *VEGFA* or sphingosine kinase (*SPHK1)*, which catalyzes S1P production, and injected them intravenously 4 and 7 days after cardiac ischemia/reperfusion in mice. Sequential delivery by transduced BM cells of VEGFA and S1P led to increased endothelial cell numbers and shorter extravascular distances in the infarct zone which support better oxygen diffusion 28 days post-MI as shown by automated 3D image analysis of the microvasculature. Milder effects were observed in the remote zone together with increased proportion of capillaries. BM cells delivering VEGFA and S1P also decreased myofibroblast abundance and restricted adverse cardiac remodeling without major impact on cardiac contractility. Our results indicate that BM cells engineered to sequentially deliver VEGFA/S1P angiogenic factors may constitute a promising strategy to improve micro-vascularization and oxygen diffusion thus limiting the adverse consequences of cardiac ischemia.

Introduction

Cardiovascular disease (CVD) has been the leading cause of death in the US since the beginning of the 20th century with almost half of those caused by coronary heart disease[1, 2]. The most common long-term consequence of coronary heart disease is heart failure (HF) and its prevalence has increased between 2009 and 2014, in part due to the improvement in acute treatment of cardiovascular disease[2]. One of the clinical manifestations of coronary heart disease is myocardial infarction (MI) which is the sudden death of myocardial tissue from ischemia caused by a blockage of a coronary artery, usually from the rupturing of an atherosclerotic plaque [3]. MI causes cardiomyocyte death, which triggers acute inflammation, angiogenesis and finally scar formation[4]. Fibrotic scar formation is the main healing mechanism after MI, due to the limited ability of the adult mammalian heart to regenerate [3]. Fibrosis causes abnormalities in both relaxation and contractility of the heart muscle, which causes ventricular remodeling, a mechanism of heart adaptation to adverse stimuli [5]. Remodeling includes left ventricle wall thinning, ventricle dilation, and changes in its shape from ellipsoid to more spherical [6]. At the cellular level, cardiomyocytes in the viable myocardium undergo hypertrophy triggered by increased load . These malformations create increasing wall stress, which causes higher myocardial oxygen demand and could cause further enlargement of the area at risk for ischemia [7]. Pathological heart remodeling caused by MI and secondary hypoxia induces HF and high mortality in the long term [8]. Indeed, HF becomes the main cause of death of patients >65 years-old within 6 years after MI[9]. HF can also derive from other CVD involving microvascular dysfunction and tissue hypoxia as hypertensive cardiac hypertrophy and diabetic coronary microangiopathy[10]. For that reason, prevention and ameliorating effects of HF are of great importance.

Over the past decades, a need for an effective therapy to prevent and limit hypoxia-related cardiac adverse remodeling and as a consequence HF, particularly after MI, remains unmet. Since the introduction of fibrinolysis and angioplasty in the late '70s, acute treatment of MI has improved dramatically, although the mortality rate caused by CVD remains high[11]. Trying to overcome the inability of adult cardiac muscle

to regenerate, many therapies were implemented, including cell and gene therapies and delivery of cytokines and soluble factors. One of the aims of these therapies has been modulating angiogenesis [12-18] since by preserving the microvasculature or boosting the formation of new vessels, tissue oxygenation would improve alleviating adverse consequences of acute or chronic ischemia. In recent years, importance has also been given to modulating immune response after MI for its beneficial effect on heart repair[19-22].

One of the main unsolved questions in these studies was the optimal delivery route for the factors with strategies including delivery of the recombinant protein [23, 24], gene delivery using plasmids [16, 17] and modified RNA[25], and virus-based approaches, mostly using AAV [14, 26, 27]. On the other hand, cell therapies, whose main effect is believed to be based on secreting factors such as VEGF and PDGF showed limited long-term improvement in cardiac vascularization[28-30]. We hypothesized that combining two approaches by delivering cells but also transducing them to overexpress proangiogenic factors may bring an improvement in cardiac vascularization after ischemia. In the field of proangiogenic therapies, the strong proangiogenic factor vascular endothelial growth factor A (VEGFA) generated promising results in animal models but showed no sustained improvement in myocardial perfusion measured in NORTHERN clinical trial[13]. However, co-delivery of VEGFA and sphingosine-1-phosphate (S1P) by AAV promoted angiogenesis and reduced cell apoptosis in a pig model of MI [14]. Of note, sequential instead of simultaneous exposure to VEGFA and S1P led to the formation of more stable vessels in scaffolds *in vitro* but this approach has never been tested *in vivo*[31].

Here we investigated the effect of bone marrow cells engineered to produce VEGFA or S1P and injected sequentially in improving vascularization in a preclinical mouse model of acute ischemic heart disease. Indeed, we demonstrate that lentiviral vector (LV)-transduced bone marrow (BM) cells injected intravenously in mice to sequentially deliver the pro-angiogenic factors VEGFA and S1P resulted in sustained increased vascularization 28 days after myocardial infarction assessed by a newly-implemented pipeline for automatized 3D image analysis of the microvasculature[32] and in contrast to the transient effect reported for non-transduced bone marrow cells. As a consequence, the strategy also limited fibrosis and

adverse cardiac remodeling. Our study may offer new therapeutic possibilities for patients suffering cardiac ischemic disease.

Materials & Methods

All experimental procedures are explained in detail in Supplemental Methods and Materials.

Lentiviral vector construction and evaluation

Human *VEGFA* and *SPHK1,* and *GFP* cDNAs were amplified by PCR and inserted downstream to the SFFV promoter of the SFFV.insert.WPRE LV backbone described in [33]. ELISA kits were used to quantify VEGFA protein level in cell supernatants. LV transduction of BM cells was performed overnight at multiplicity of infection (MOI) 50. The collection of cell supernatant was performed 48h and 72h after transduction. S1P expression was measured by mass spectrometry 48h after infection with LV_S PHK1. For further details, see Supplemental Methods.

Flow cytometry

BM cells were stained with antibodies against CD11b- AF647, F4/80-PE-Cy7, Ly6C-FITC, CCR2-PE and CX_3CR1-Pacific Blue and 7-AAD live/death dye. Sample acquisition was performed using a flow cytometer BD LSRFortessa and analyzed using FlowJo software. Detailed staining procedure and a list of antibodies is available in Supplemental Methods.

Aortic ring assay

Aortic ring assay was performed as described in [34]. Mouse aortic rings were cultured in the presence of various combinations of soluble factors (rhVEGF 30ng/ml, S1P 1µM) or mouse BM cells previously transduced with LVs (BM ^{hVEGF}, BM ^{SPHK1}). At day 8 rings were fixed in 1.6% PFA, and incubated overnight at 4℃ with the following antibodies/reagents: IB4 or anti-CD31 (1:150) for endothelial cells and anti-SMA (1:400) for mural cells. Images were acquired with a Nikon A1R confocal system coupled to a Nikon Ti-Eclipse microscope using a 10x objective and capturing 400µm in depth with a z-stack every 3µm. Analysis of aortic ring images was performed using Imaris software and a Matlab-based method for 3D-microvasculature developed in our lab. Reagents, antibodies and detailed procedures are described in

Supplemental Methods.

In vivo mouse I/R experiment protocol

Mice were kept at the Animal facility of CNIC under specific pathogen-free conditions and in accordance with the institutional guidelines. Animal procedures were approved by the corresponding legal authority of the local government of Madrid (reference number of approval PROEX/ 34/13). I/R was performed in 10-12 week old male BL6 mice by ligation of left anterior descendent coronary artery for 45 min ischemia followed by reperfusion. Echocardiography was performed 3 days after to confirm myocardial infarction and mice with LVEF between 20-40 % were randomly assigned to control and treated groups. Four days post I/R, mice were intravenously injected with $5x10^6$ BM^{hVEGF} in 100µl of PBS or with PBS only as a control. Seven days post I/R, a second injection was performed, with $5x10^6$ BM^{hSPHK1} or PBS. At day 28, after endpoint echocardiography, hearts were weighed and collected. Echocardiography was performed using Vevo 2100 Ultra High Frequency ultrasound to assess cardiac parameters (end-diastolic and end-systolic volumes, stroke volume and left ventricular ejection fraction and left ventricle posterior wall thickness). Analysis of heart roundness (i.e. sphericity) was performed on macroscopic images of the dissected hearts using ImageJ [35] software. Fibrosis was assessed based on Masson-Trichrome staining of series of seven levels of tissue cuts starting from the apex to the base of the heart and visualized using NanoZoomer-2.ORS® (Hamamatsu); scar area is represented as the percentage of LV area using ImageJ software. To quantify cardiomyocyte size, ImageJ based semi-automated macro was designed where cardiomyocytes were recognized by laminin staining and their area and perimeter quantified. Detailed experimental procedures are described in Supplemental Methods.

Microvasculature analysis

Sections of 15µm were stained with anti-CD31, anti-PDGFR□, and anti-SMA antibodies and with Hoechst for nuclear staining. Images were acquired with a Leica SP5 confocal microscope using a 40x objective (NA 1.25) with oil immersion with z-stacks captured every 1µm. The analysis of the microvasculature has been based on the fully automatic image analysis pipeline developed in our laboratory to analyze

microvascular data. The pipeline permits the calculation of a pool of parameters that quantify all major features of the vascular network. It has been described in detail in [32], while a brief overview of necessary adaptations is provided in Supplemental Methods.

Statistics

Statistical analysis was performed using GraphPad Prism 6/7 software. Distribution of the data sets were checked with D'Agostino-Pearson and Shapiro–Wilk normality tests, and then parametric or non-parametric tests were performed as indicated in the legends. Outliers were identified using the ROUT method (Q=1.000%). P-values were defined as follows: *<0.05; **<0.01; *** < 0.001, ****< 0.0001. Sample size (n) is indicated in each figure.

Results

Experimental design for *in vivo* sequential VEGF/S1P gene-cell angiotherapy in a MI mouse model

Sequential delivery of VEGFA (VEGF hereafter) and S1P has been shown to increase the formation of mature vessels in *in vitro* scaffolds compared to the effect of single or combined factors[31]. We confirmed in the mouse aortic ring assay that sequential delivery of S1P after VEGF or combined delivery of the two factors induced a significantly higher proportion of sprouts, covered by smooth muscle actin (SMA)-positive cells, and a more complex vascular network than VEGF alone (**Figure S1A and S1B**). We therefore decided to test the effects of a combined gene-cell therapy in which BM cells were boosted to produce VEGF and S1P by LV-transduction and deliver these factors sequentially. For that, we generated LVs encoding for the human *VEGFA*, or *SPHK1* (sphingosine-kinase 1), the enzyme which catalyzes the conversion of the precursor sphingolipid sphingosine to the active form S1P, hereon LV_hVEGF, and LV_hSPHK1 respectively. We then validated the efficacy of the LV in HEK and mouse BM cells transduced with LV_hVEGF, and LV_hSPHK1 which indeed overexpressed VEGFA, and produced S1P (**Figure S2**). We tested the proposed strategy in the mouse model of acute cardiac ischemia/reperfusion which is closer to the human MI clinical practice. Before proceeding with the *in vivo* approach, we confirmed the ability of intravenously injected BM cells to migrate to the infarcted myocardium. Histological analysis performed 24h after Tomato^{+} BM cell i.v. injection confirmed the presence of red round cells in the infarct zone of hearts 4 days after ischemia/reperfusion; only unspecific non-membrane-associated red signal was detected in hearts from PBS-injected mice **(Figure S3A**).

Prior to their i.v. injection we also analyzed whether LV transduction and culture in the presence of stem cell factor (SCF) and M-CSF *in vitro* impacted on the phenotype of BM cells. Following the flow cytometry gating strategy detailed in M&M section (**Figure S3B-C**), we observed that after LV transduction with LV_hVEGF or LV_hSPHK1 the amount of neutrophils increased, macrophages decreased and the scarce myeloid progenitors remained unchanged (**Figure S3D-F**). Notably, although no

differences in the percentage of monocytes (~60%) were observed, after LV transduction there was an increase in their CX_3CR1 cell surface expression, particularly after LV_hSPHK1 transduction with milder changes in CCR2 levels **(Figure S3G**).

BM cell-mediated delivery of VEGF and S1P improves vascularization and reduces inter-capillary distances in the post-infarcted heart

We then tested the *in vivo* impact of boosting BM cell sequential secretion of VEGF and S1P in a mouse model of cardiac ischemia/reperfusion (I/R) (**Figure S4A).** MI was confirmed by echocardiography 3 days post-I/R and mice with LVEF 20-40% were included in the study. Mice were afterwards randomly assigned to control and treated groups, and then injected intravenously at day 4 post-I/R with PBS or with $5x10^6$ of BM^{hVEGF} followed at day 7 by PBS or $5x10^6$ of BM^{hSPHK1} similarly to the time-points tested in the *in vitro* aortic ring assay (**Figure S1**).

Sequential VEGF/S1P angiotherapy by BM cells was primarily designed to enhance angiogenesis and increase the functional microvasculature after I/R which may secondarily reduce post-MI adverse effects. In an effort to quantify the effect of the proposed treatment to the microvasculature in an unbiased and reproducible manner, we analyzed images of transverse slices of cardiac tissue from treated and untreated subjects by means of a 3D fully automated image analysis pipeline developed at our lab [32]. The tissue was labeled for blood vessels, in particular for endothelial cells (CD31) and for smooth muscle actin (SMA) and PDGFR□-positive cells, and then imaged by confocal microscopy. The automated analysis approach allowed us to compare the post-MI changes of the microvasculature of the control and BM cell-delivered VEGF/S1P hearts in terms of all major microvascular characteristics; morphology, topology, angio-architecture, efficiency for oxygen diffusion, as well as its relation with SMA^+ and PDGFR□$^+$ cells. A summary of all quantified parameters and their changes is provided in **Table 1**. In the same table, reference values for the parameters extracted from microvascular tissues of basal mice are given.

Among fractal parameters, lacunarity, a parameter measuring the heterogeneity in the distribution of the

size of the gaps in the tissue, significantly decreased in the infarcted area of the hearts in the treated group. This indicates a smaller dispersion of non-vascularized areas implying a better-organized microvasculature (**Table 1**). Although no significant differences were observed in the overall vascular volume density 28 days after I/R, after decomposing the microvasculature into its components, i.e. capillaries ($CD31^+SMA^-$ < 5 μm), enlarged capillaries ($CD31^+SMA^-$, > 5.1 μm) and arterioles ($CD31^+SMA^+$), we noticed a trend to increased capillary volume density and decreased enlarged capillaries in the infarcted zone of hearts from mice injected with BM cells delivering VEGF/S1P compared to controls (**Figure 1A-C and Table 1**). There were however no changes in the volume density and the percentage of arterioles (**Figure 1B-C**). Accordingly, treatment also resulted in significantly more abundant endothelial cells in the vasculature of the infarcted zone (**Figure 1A**). Interestingly, in the remote zone, we also observe a significant increase in the volume and percentage of capillaries and a decrease in the percentage of enlarged capillaries in hearts from the VEGF/S1P-treated group in spite of the lack of statistically significant between-group differences in overall vascular volume density. Concomitantly, endothelial cell abundance in the remote zone was slightly increased in the treated group (**Figure 1D-F**). These findings indicate that combined delivery of VEGF/S1P impacted mostly on the capillaries increasing their volume density and the endothelial cell content while decreasing their remodeling/enlargement in both the infarcted and the remote zones.

The main function of the microvasculature is to provide nutrients and oxygen to the heart, particularly after ischemia, to preserve cell viability and promote repair. Thus, towards obtaining insights into the efficiency of the network for oxygen diffusion, we studied by means of our automated pipeline traditional indicators of oxygen diffusion, i.e. maximal extravascular distances. Accordingly to the larger proportion of capillaries and higher endothelial cell numbers, maximal extravascular distances were significantly reduced in the infarct zone of hearts from mice injected with BM cells producing VEGF and S1P 28 days after I/R compared to the controls indicating better oxygen diffusion; a similar trend to reduced extravascular distances was observed in the remote zone of treated mice (**Figure 2**).

We next sought to decipher the contribution of VEGF and S1P overexpression versus endogenous

secretion of factors by BM cells to the myocardial angiogenic phenotype since PBS was used as *in vivo* control. Non-transduced BM cells did not increase vascular sprouting versus control medium in the aortic ring in contrast to sequential exposure to BM cells secreting VEGF and S1P which induced a significant increase in vascular sprouts with a good proportion covered by SMA-positive cells, indicative of stable vessels, and a more complex vascular network (**Figure S4 B**). These findings argue in favor of overexpressed VEGF and S1P by LV-transduced BM cells as the factors responsible for boosting capillarization post-MI.

Sequential BM cell delivery of VEGFA and S1P diminishes post-infarction tissue fibrosis with no impact on cardiac contractility

After myocardial infarction, dead cardiomyocytes are mostly replaced by fibrotic tissue reducing cardiac pump function. We analyzed whether improved capillarization and oxygen diffusion by BM cell sequential delivery of VEGF/S1P had any impact on cardiomyocyte survival and thus in cardiac performance. Despite the presence of isolated clusters of viable cardiomyocytes within the scar of infarcted hearts from VEGF/S1P-treated mice but not in untreated controls 28 days post-I/R (**Figure S5A**), echocardiography analysis showed no significant between-group differences in the reduced left ventricle ejection fraction (LVEF) and the stroke volume (SV) (**Figure S5B-C**).

Regardless the ejection fraction values, fibrosis extent and tissue stiffness are the major factors driving post-MI progression to heart failure. Therefore, although we could not observe a major impact of the BM cell-VEGF/S1P therapy on cardiac contractility, we next assessed fibrosis-related parameters since cardiac injury and hypoxia are enhancers of the myofibroblast-driven fibrotic program[36, 37]. We could not detect between-group differences in the total scar volume of the left ventricle free wall calculated from serial Masson stained-sections spanning the whole heart 28 days post-I/R (**Figure 3A, B**); the cardiac section closest to the valves consistently showed however a significantly reduced scar area in the BM cell VEFG/S1P-treated group (**Figure 3 C**). Complementarily, using the images of mouse cardiac tissues

stained for PDGFRα and CD31, we also automatically quantitated the myofibroblast abundance as the ratio of the volume of myofibroblasts over the volume of all PDGFRα-positive cells. In this approach, myofibroblasts are considered PDGFRα positive areas that are not in touch with the vessels [32,38]. Following this approach, we noticed significantly reduced myofibroblast abundance in the infarct zone of hearts from BM cell VEGF/S1P-treated mice compared to untreated controls; myofibroblasts were barely detected but fewer in the remote zone of the treated group (**Figure 3D, E and Table 1**). Since myofibroblasts are in charge of secreting and remodeling extracellular matrix proteins, particularly collagens, to form the scar, myofibroblast reduction prompted us to analyze collagen fiber organization and condensation in spite of no significant differences observed in overall scar area. Analysis of first order features of collagen fibrils in second harmonic generation microscopy images revealed increased skewness and kurtosis in the collagen fibers of the scar from infarcted hearts of the BM cell VEGF/S1P-treated group compared to controls (**Figure 3F, G**); these values would indicate thinner and underdeveloped collagen fibers and thus lower tissue stiffness[39].

VEGFA and S1P sequential delivery by BM cells limits adverse cardiac remodeling post-MI

One of the consequences of MI is cardiac remodeling defined as the post-damage alterations which result in acute and chronic changes of heart size, mass, geometry and function which may finally lead to cardiac dysfunction and HF[40]. We first quantitated ventricle cavity size and wall thickness and observed a trend to reduced dilatation and thickening of the left ventricle in the VEGF/S1P-treated mice 28 days post I/R (**Figure 4A, B**). Since volume and thickness changes are not fully developed 4 weeks after I/R in mice [41], we also analyzed global cardiac geometry which is modified more acutely [40]. We found that hearts from BM cell VEGF/S1P-treated mice kept their ellipsoid-like shape in contrast to those from untreated control mice that became significantly rounder at 28 days post-I/R as expected (**Figure 4C**). Moreover analysis of cardiomyocytes in the remote zone which usually become hypertrophic in response to post-MI left ventricle stiffness and volume overload [40], showed that cardiomyocytes in the remote zone of hearts from

BM cell VEGF/S1P-treated mice became less hypertrophic with significantly smaller area and perimeter compared with control mice 28 days post-I/R (**Figure 4D, E)**. Finally, cardiac remodeling also results in changes at the molecular level with proteins increasing (collagen type I) or decreasing (Atpa2a/Serca2a) during the process[40]. Notably, VEGF/S1P-treatment led to decreased collagen type I and increased Atp2a2 (Serca2) protein levels in heart extracts compared to untreated mice 28 days post-I/R (**Figure 4F, G**), confirming that the angiotherapy ameliorated adverse cardiac remodeling[40].

Collectively these findings indicate that sequential VEGFA/S1P gene- BM cell therapy limits post-MI adverse cardiac remodeling consistent with the enhanced capillarization and oxygen diffusion effects and reduced myofibroblast abundance in the infarcted tissue.

Discussion

In this study, we tested the effect of sequential delivery by BM cells of the proangiogenic factors VEGF and S1P on boosting angiogenesis and/or preserving the microvasculature after MI in vivo. The intervention succeeded in increasing endothelial cell numbers and capillaries and diminishing adverse angioadaptation, thus improving oxygen diffusion 4 weeks after the ischemic event. In spite of no major effect on cardiac contractility, BM cell sequential VEGF/S1P therapy also reduced myofibroblast-driven tissue fibrosis and limited adverse post-MI cardiac remodeling.

In terms of safety and possible translation of this therapy, LV transduction is performed *ex vivo* and the injected cells are mostly differentiated. This would limit the possibility of transferring the LV to other cell types in the organism and reduce risks of genetic alterations in the hematopoietic progenitors and their progeny by LV insertion. Our previous analysis in the pig infarcted heart has shown that at day 3 post-MI the 3D structure of the microvasculature is mostly preserved but its function starts to decline as manifested by the larger extravascular distances causing disturbed oxygen diffusion [32]. Endogenous angiogenesis after MI occurs during the first two weeks after the ischemic event. Thus, detailed kinetics of the endothelial cell marker PECAM1/CD31 in a mouse model of permanent coronary artery ligation showed an increase in endothelial cells at 2 days with a maximum at 4 days and then a decline and return to baseline levels 7 days after MI[4, 36, 42,43]. These findings support our vascular boosting intervention 4 days post-MI.

In our study, we analyzed the impact of the BM cell VEGF/S1P therapy at 28 days end-point post-I/R. Notably we observed persistent benefits from this strategy in contrast to previously reported therapeutic approaches in which effects on the vasculature were often transient. For example, the intramyocardial injection of mesenchymal stem cells showed benefits in perfusion on the infarcted area at the first week but not after 4 weeks [44]. This newly implemented BM cell VEGF/S1P therapy mainly induced an increase in the abundance of endothelial cells and reduced extravascular distances in the infarcted area of hearts from treated mice. Concomitantly, trends towards decreased presence of enlarged capillaries were

observed. These effects might indicate reduced angioadaptation which normally occurs in response to capillary loss and flow redistribution in the remaining vessels [32, 45]. Previous proangiogenic therapies, including AAV-mediated overexpression of VEGF and ANG 1 in a pig model of MI[14], plasmid-mediated overexpression of bFGF and PDGF in a rat model of MI[46], and microcapsule release of FGF2 and HGF in a rat model of HF [47], improved the cardiac vasculature by increasing both capillary and arteriole/large vessel content. As it is becoming recently accepted, interventions in the cardiac stroma [48] as the microvasculature may secondarily lead to reduced CM death, tissue damage and fibrosis since this is often triggered by tissue hypoxia[37].

We based our intervention on previous reports showing that sequential VEGF and S1P actions were of benefit to induce stable vessels in scaffolds *in vitro* [31]. VEGF is a proangiogenic factor, which induces endothelial cell migration, proliferation and survival depending on the endothelial cell context and at high persistent levels may induce vascular leakiness and regression[49, 50]. The increase in endothelial cell number in the infarcted area of hearts from treated mice suggests an overall effect of VEGF in endothelial cell proliferation and/or survival. Moreover, stimulation of endothelial cells with VEGF causes overexpression of S1P1 receptors on these cells; and in isolated arteries, enhances S1P-mediated vasorelaxation and eNOS phosphorylation[31]. This effect may contribute further to pro-survival and proangiogenic programs in the capillary endothelium. It is worth mentioning that although VEGF and S1P are endogenously produced in the heart, cell-type transcriptomics analysis in the pig heart revealed decreased mRNA levels of VEGF and SPHK1 3 days post-I/R (our unpublished data), supporting the rationale of boosting VEGF/S1P tissue levels by LV-BM delivery. S1P itself is considered a master regulator of signaling pathways involved in cardiac improvement after MI and it has lately attracted attention as a possible target[51]. We cannot rule out that S1P secreted locally by the transduced BM cells in the infarcted area could have, in addition to enhanced capillarization, some direct impact on cardiomyocyte survival and, thus, on reducing cardiac damage. Nonetheless, the lack of major differences in the infarct size argues against a major role of this protection mechanism. Furthermore, in contrast to the reported S1P effect on myofibroblasts[51], we observe

reduced myofibroblast abundance suggesting that S1P paracrine effects on cell types other than endothelial cells seem unlikely. Autocrine effects however may still be possible since transduction with LV_hVEGF or LV_hSPHK1 resulted in BM-derived monocytes with higher CX_3CR1 levels, which may enhance their early traffic to the damaged heart [52]. In this line, higher expression of the CX_3CR1 receptor on circulating $Ly6C^{low}$ monocytes has been shown to induce a positive effect on their recruitment and the promotion of angiogenesis in the injury site in hind limb ischemia [53] and carotid injury [54] models. Moreover, S1P can promote an anti-inflammatory phenotype in macrophages through activation of their S1P1 receptor after damage and contribute to macrophage-mediated cardiac repair[55]; this possibility will deserve further analysis with macrophage specific markers. Of note, significantly increased capillaries and a trend to diminished extravascular distances were also observed in the remote zone of BM cell VEGF/S1P treated infarcted mice suggesting that LV-BM cells can induce vascular effects also in that area[56].

VEGF/S1P gene-cell therapy did not improve post-MI cardiac contractility in accordance with other previously reported strategies. Nevertheless, in spite of no major impact on contractility, VEGF/S1P combined angiotherapy limited post-MI adverse cardiac remodeling as demonstrated by the preserved cardiac geometry and cardiomyocyte morphology in the remote zone as well as the higher Atp2a2 protein levels. The reduced cardiac sphericity induced by the angio therapy supports its clinical relevance since it has been related to post-MI long term survival[57]. This improvement may be related to the reduced collagen stiffness and myofibroblast abundance in the infarcted area but also in the remote zone of hearts from the treated mice[58]; whether remote changes are directly related to the therapy, or indirect as a consequence of the effects on the scar properties (better perfusion, lower stiffness) in the infarcted area remains to be elucidated. Moreover, since cardiac macrophages proliferate in response to mechanical stretching caused by stiffer failing myocardium[20], the reduced collagen stiffness in treated mice may also explain the trend to lower amount of macrophages in the remote zone observed in these mice (unpublished data).

There were fewer functional beneficial effects of the angio therapy than expected, despite a consistent biological effect on histology endpoints. This may be related to insufficient factor concentration in the *in*

vivo experiments, and more dramatic effect needs to be induced to elicit relevant functional changes. In this regard, future studies with higher transgene overexpression, or more effective gene-cell delivery systems (intracoronary, trans-endocardial) may overcome the limitations we observed in the murine model[59].

Our work presents some limitations, which will deserve future studies. First, in our study, gene-cell therapy was compared to a placebo to acquire a clear determination of its efficacy. Although the absence of angiogenic effects induced by non-transduced BM cells on the mouse aortic rings argue in favor of specific effects of sequential delivery of VEGF plus S1P on the phenotype observed in the microvasculature 28 days post-MI, comparison with injection of wild-type or LV mock-transduced BM cells would help establish the precise contribution of paracrine signaling by the BM cells versus the delivered VEGF/S1P in vivo. Second, deciphering the actual impact of the combined gene-cell VEGF and S1P therapy on the microvasculature, cardiomyocyte survival and/or monocyte/macrophage subsets will require deeper analysis at earlier time-points after ischemia. Third, we have only been tested the benefits of this strategy in the I/R model by its proximity to the clinical practice. It will also be of interest to evaluate the impact of combined VEGF/S1P gene-cell therapy in the extensively used permanent LAD coronary artery ligation in which arterialization is relevant for revascularization as well as in CVD involving chronic cardiac ischemia. Forth, in terms of global cardiac function, clinical trials using intracoronary injection of whole BM showed no long-term improvement in LVEF after MI [60, 61], despite promising short-term effects [62, 63]. Therefore, analysis of the impact of BM cell VEGF/S1P therapy at longer time-points after cardiac ischemia is guaranteed to understand whether the beneficial effects on cardiac remodeling persist in time.

In sum, our study offers a novel therapeutic strategy based on sequential BM cell delivery of angiogenic factors to enhance micro-vascularization and oxygen diffusion thus limiting the adverse consequences of cardiac ischemic diseases.

Acknowledgments

We thank Mónica Gómez for her help with I/R surgery, Lorena Flores and Ana Vanessa Alonso López for performing and analyzing echocardiography, Dr. Manuel Lobo for ultrasound image analysis, Dr. Borreguero and Dr. Maria Villalba for their help in interpreting the results, and Verónica Labrador and CNIC's Microcopy Unit for their expertise and help with image analysis.

Funding

This study was supported by grants from the Spanish Ministerio de Ciencia, Innovación y Universidades SAF2014-52050-R and SAF2017-83229-R to A.G.A. and BIO2015-67580-P to J.V.) and the Carlos III Institute of Health-Fondo de Investigación Sanitaria (PRB2, IPT13/0001-ISCIII-SGEFI/FEDER, ProteoRed). The research leading to these results has received funding from the People Programme (Marie Curie Action) of the European Union's Seventh Framework Programme (FP7/2007-2013) under REA grant Agreement 608027. The CNIC is supported by the Spanish Ministerio de Ciencia, Innovación y Universidades and the Pro-CNIC Foundation, and is a Severo Ochoa Center of Excellence (award SEV-2015-0505).

Author contribution

M.M.Ż. designed and performed the experiments, analyzed the results, and wrote the manuscript; P.G. performed image analysis of the microvasculature and contribute critical suggestions; C.C. performed and analyzed western blot and immunostaining experiments; R.A.M. performed mouse surgeries; M.L.S. and M.D.P. provided the lentiviral backbone and expertise with cloning; A.F. and J.V. performed and analyzed S1P measurements; S.R. helped with LV cloning; J.A. provided conceptual critical suggestions to the manuscript; E.O. and B.I. coordinated mouse surgeries and ultrasound analysis and provided advice; A.G.A. conceived and supervised the project and wrote the manuscript.

Reference

1. Mendis S, Puska P, Norrving B, World Health Organization., World Heart Federation. and World Stroke Organization. Global atlas on cardiovascular disease prevention and control. Geneva: World Health Organization in collaboration with the World Heart Federation and the World Stroke Organization; 2011.
2. Benjamin EJ, Blaha MJ, Chiuve SE, Cushman M, Das SR, Deo R, de Ferranti SD, Floyd J, Fornage M, Gillespie C, Isasi CR, Jimenez MC, Jordan LC, Judd SE, Lackland D, Lichtman JH, Lisabeth L, Liu S, Longenecker CT, Mackey RH, Matsushita K, Mozaffarian D, Mussolino ME, Nasir K, Neumar RW, Palaniappan L, Pandey DK, Thiagarajan RR, Reeves MJ, Ritchey M, Rodriguez CJ, Roth GA, Rosamond WD, Sasson C, Towfighi A, Tsao CW, Turner MB, Virani SS, Voeks JH, Willey JZ, Wilkins JT, Wu JH, Alger HM, Wong SS and Muntner P. Heart Disease and Stroke Statistics-2017 Update: A Report From the American Heart Association. Circulation. 2017;135:e146-e603.
3. Frangogiannis NG. Pathophysiology of Myocardial Infarction. Compr Physiol. 2015;5:1841-75.
4. Matsui Y, Morimoto J and Uede T. Role of matricellular proteins in cardiac tissue remodeling after myocardial infarction. World J Biol Chem. 2010;1:69-80.
5. Schirone L, Forte M, Palmerio S, Yee D, Nocella C, Angelini F, Pagano F, Schiavon S, Bordin A, Carrizzo A, Vecchione C, Valenti V, Chimenti I, De Falco E, Sciarretta S and Frati G. A Review of the Molecular Mechanisms Underlying the Development and Progression of Cardiac Remodeling. Oxid Med Cell Longev. 2017;2017:3920195.
6. Jessup M and Brozena S. Heart failure. N Engl J Med. 2003;348:2007-18.
7. Bhatt AS, Ambrosy AP and Velazquez EJ. Adverse Remodeling and Reverse Remodeling After Myocardial Infarction. Curr Cardiol Rep. 2017;19:71.
8. Taimeh Z, Loughran J, Birks EJ and Bolli R. Vascular endothelial growth factor in heart failure. Nat Rev Cardiol. 2013;10:519-30.
9. Torabi A, Cleland JG, Rigby AS and Sherwi N. Development and course of heart failure after a myocardial infarction in younger and older people. J Geriatr Cardiol. 2014;11:1-12.
10. Pieske B and Wachter R. Impact of diabetes and hypertension on the heart. Current opinion in cardiology. 2008;23:340-9.
11. Bennett J and Dubois C. Percutaneous coronary intervention, a historical perspective looking to the future. J Thorac Dis. 2013;5:367-70.
12. Doppler SA, Deutsch MA, Lange R and Krane M. Cardiac regeneration: current therapies-future concepts. J Thorac Dis. 2013;5:683-97.
13. Stewart DJ, Kutryk MJ, Fitchett D, Freeman M, Camack N, Su Y, Della Siega A, Bilodeau L, Burton JR, Proulx G and Radhakrishnan S. VEGF gene therapy fails to improve perfusion of ischemic myocardium in patients with advanced coronary disease: results of the NORTHERN trial. Mol Ther. 2009;17:1109-15.
14. Tao Z, Chen B, Tan X, Zhao Y, Wang L, Zhu T, Cao K, Yang Z, Kan YW and Su H. Coexpression of VEGF and angiopoietin-1 promotes angiogenesis and cardiomyocyte proliferation reduces apoptosis in porcine myocardial infarction (MI) heart. Proc Natl Acad Sci U S A. 2011;108:2064-9.
15. Hedman M, Hartikainen J, Syvanne M, Stjernvall J, Hedman A, Kivela A, Vanninen E, Mussalo H, Kauppila E, Simula S, Narvanen O, Rantala A, Peuhkurinen K, Nieminen MS, Laakso M and Yla-Herttuala S. Safety and feasibility of catheter-based local intracoronary vascular endothelial growth factor gene transfer in the prevention of postangioplasty and in-stent restenosis and in the treatment of chronic myocardial ischemia: phase II results of the Kuopio Angiogenesis Trial (KAT). Circulation. 2003;107:2677-83.
16. Kastrup J, Jorgensen E, Ruck A, Tagil K, Glogar D, Ruzyllo W, Botker HE, Dudek D, Drvota V, Hesse B, Thuesen L, Blomberg P, Gyongyosi M and Sylven C. Direct intramyocardial plasmid vascular endothelial growth factor-A165 gene therapy in patients with stable severe angina pectoris A randomized

double-blind placebo-controlled study: the Euroinject One trial. J Am Coll Cardiol. 2005;45:982-8.
17. Vera Janavel GL, De Lorenzi A, Cortes C, Olea FD, Cabeza Meckert P, Bercovich A, Criscuolo M, Laguens R and Crottogini A. Effect of vascular endothelial growth factor gene transfer on infarct size, left ventricular function and myocardial perfusion in sheep after 2 months of coronary artery occlusion. J Gene Med. 2012;14:279-87.
18. Ieda M, Fu JD, Delgado-Olguin P, Vedantham V, Hayashi Y, Bruneau BG and Srivastava D. Direct reprogramming of fibroblasts into functional cardiomyocytes by defined factors. Cell. 2010;142:375-86.
19. Nahrendorf M, Swirski FK, Aikawa E, Stangenberg L, Wurdinger T, Figueiredo JL, Libby P, Weissleder R and Pittet MJ. The healing myocardium sequentially mobilizes two monocyte subsets with divergent and complementary functions. J Exp Med. 2007;204:3037-47.
20. Sager HB, Hulsmans M, Lavine KJ, Moreira MB, Heidt T, Courties G, Sun Y, Iwamoto Y, Tricot B, Khan OF, Dahlman JE, Borodovsky A, Fitzgerald K, Anderson DG, Weissleder R, Libby P, Swirski FK and Nahrendorf M. Proliferation and Recruitment Contribute to Myocardial Macrophage Expansion in Chronic Heart Failure. Circ Res. 2016;119:853-64.
21. van den Akker F, Deddens JC, Doevendans PA and Sluijter JP. Cardiac stem cell therapy to modulate inflammation upon myocardial infarction. Biochim Biophys Acta. 2013;1830:2449-58.
22. Hamid T and Prabhu SD. Immunomodulation Is the Key to Cardiac Repair. Circ Res. 2017;120:1530-1532.
23. Lopez JJ, Laham RJ, Stamler A, Pearlman JD, Bunting S, Kaplan A, Carrozza JP, Sellke FW and Simons M. VEGF administration in chronic myocardial ischemia in pigs. Cardiovasc Res. 1998;40:272-81.
24. Henry TD, Annex BH, McKendall GR, Azrin MA, Lopez JJ, Giordano FJ, Shah PK, Willerson JT, Benza RL, Berman DS, Gibson CM, Bajamonde A, Rundle AC, Fine J and McCluskey ER. The VIVA trial: Vascular endothelial growth factor in Ischemia for Vascular Angiogenesis. Circulation. 2003;107:1359-65.
25. Zangi L, Lui KO, von Gise A, Ma Q, Ebina W, Ptaszek LM, Spater D, Xu H, Tabebordbar M, Gorbatov R, Sena B, Nahrendorf M, Briscoe DM, Li RA, Wagers AJ, Rossi DJ, Pu WT and Chien KR. Modified mRNA directs the fate of heart progenitor cells and induces vascular regeneration after myocardial infarction. Nat Biotechnol. 2013;31:898-907.
26. Pacak CA, Mah CS, Thattaliyath BD, Conlon TJ, Lewis MA, Cloutier DE, Zolotukhin I, Tarantal AF and Byrne BJ. Recombinant adeno-associated virus serotype 9 leads to preferential cardiac transduction in vivo. Circ Res. 2006;99:e3-9.
27. Vassalli G, Bueler H, Dudler J, von Segesser LK and Kappenberger L. Adeno-associated virus (AAV) vectors achieve prolonged transgene expression in mouse myocardium and arteries in vivo: a comparative study with adenovirus vectors. Int J Cardiol. 2003;90:229-38.
28. Kocher AA, Schuster MD, Szabolcs MJ, Takuma S, Burkhoff D, Wang J, Homma S, Edwards NM and Itescu S. Neovascularization of ischemic myocardium by human bone-marrow-derived angioblasts prevents cardiomyocyte apoptosis, reduces remodeling and improves cardiac function. Nat Med. 2001;7:430-6.
29. Bartunek J, Vanderheyden M, Vandekerckhove B, Mansour S, De Bruyne B, De Bondt P, Van Haute I, Lootens N, Heyndrickx G and Wijns W. Intracoronary injection of CD133-positive enriched bone marrow progenitor cells promotes cardiac recovery after recent myocardial infarction: feasibility and safety. Circulation. 2005;112:I178-83.
30. Takahashi M, Li TS, Suzuki R, Kobayashi T, Ito H, Ikeda Y, Matsuzaki M and Hamano K. Cytokines produced by bone marrow cells can contribute to functional improvement of the infarcted heart by protecting cardiomyocytes from ischemic injury. Am J Physiol Heart Circ Physiol. 2006;291:H886-93.
31. Tengood JE, Kovach KM, Vescovi PE, Russell AJ and Little SR. Sequential delivery of vascular endothelial growth factor and sphingosine 1-phosphate for angiogenesis. Biomaterials. 2010;31:7805-12.
32. Gkontra P, Norton KA, Zak MM, Clemente C, Aguero J, Ibanez B, Santos A, Popel AS and Arroyo AG. Deciphering microvascular changes after myocardial infarction through 3D fully automated

image analysis. Sci Rep. 2018;8:1854.
33. Squadrito ML, Pucci F, Magri L, Moi D, Gilfillan GD, Ranghetti A, Casazza A, Mazzone M, Lyle R, Naldini L and De Palma M. miR-511-3p modulates genetic programs of tumor-associated macrophages. Cell Rep. 2012;1:141-54.
34. Baker M, Robinson SD, Lechertier T, Barber PR, Tavora B, D'Amico G, Jones DT, Vojnovic B and Hodivala-Dilke K. Use of the mouse aortic ring assay to study angiogenesis. Nat Protoc. 2011;7:89-104.
35. Schindelin J, Arganda-Carreras I, Frise E, Kaynig V, Longair M, Pietzsch T, Preibisch S, Rueden C, Saalfeld S, Schmid B, Tinevez JY, White DJ, Hartenstein V, Eliceiri K, Tomancak P and Cardona A. Fiji: an open-source platform for biological-image analysis. Nat Methods. 2012;9:676-82.
36. Prabhu SD and Frangogiannis NG. The Biological Basis for Cardiac Repair After Myocardial Infarction: From Inflammation to Fibrosis. Circ Res. 2016;119:91-112.
37. Talman V and Ruskoaho H. Cardiac fibrosis in myocardial infarction-from repair and remodeling to regeneration. Cell Tissue Res. 2016;365:563-81.
38. Fan H, Ma L, Fan B, Wu J, Yang Z and Wang L. Role of PDGFR-beta/PI3K/AKT signaling pathway in PDGF-BB induced myocardial fibrosis in rats. Am J Transl Res. 2014;6:714-23.
39. Mostaco-Guidolin L, Rosin NL and Hackett TL. Imaging Collagen in Scar Tissue: Developments in Second Harmonic Generation Microscopy for Biomedical Applications. Int J Mol Sci. 2017;18.
40. Azevedo PS, Polegato BF, Minicucci MF, Paiva SA and Zornoff LA. Cardiac Remodeling: Concepts, Clinical Impact, Pathophysiological Mechanisms and Pharmacologic Treatment. Arq Bras Cardiol. 2016;106:62-9.
41. De Celle T, Cleutjens JP, Blankesteijn WM, Debets JJ, Smits JF and Janssen BJ. Long-term structural and functional consequences of cardiac ischaemia-reperfusion injury in vivo in mice. Exp Physiol. 2004;89:605-15.
42. Silvestre JS, Smadja DM and Levy BI. Postischemic revascularization: from cellular and molecular mechanisms to clinical applications. Physiol Rev. 2013;93:1743-802.
43. Dube KN, Thomas TM, Munshaw S, Rohling M, Riley PR and Smart N. Recapitulation of developmental mechanisms to revascularize the ischemic heart. JCI Insight. 2017;2.
44. Schuleri KH, Amado LC, Boyle AJ, Centola M, Saliaris AP, Gutman MR, Hatzistergos KE, Oskouei BN, Zimmet JM, Young RG, Heldman AW, Lardo AC and Hare JM. Early improvement in cardiac tissue perfusion due to mesenchymal stem cells. Am J Physiol Heart Circ Physiol. 2008;294:H2002-11.
45. Zakrzewicz A, Secomb TW and Pries AR. Angioadaptation: keeping the vascular system in shape. News Physiol Sci. 2002;17:197-201.
46. Hao X, Mansson-Broberg A, Gustafsson T, Grinnemo KH, Blomberg P, Siddiqui AJ, Wardell E and Sylven C. Angiogenic effects of dual gene transfer of bFGF and PDGF-BB after myocardial infarction. Biochem Biophys Res Commun. 2004;315:1058-63.
47. Banquet S, Gomez E, Nicol L, Edwards-Levy F, Henry JP, Cao R, Schapman D, Dautreaux B, Lallemand F, Bauer F, Cao Y, Thuillez C, Mulder P, Richard V and Brakenhielm E. Arteriogenic therapy by intramyocardial sustained delivery of a novel growth factor combination prevents chronic heart failure. Circulation. 2011;124:1059-69.
48. Forte E, Furtado MB and Rosenthal N. The interstitium in cardiac repair: role of the immune-stromal cell interplay. Nat Rev Cardiol. 2018;15:601-616.
49. Baluk P, Lee CG, Link H, Ator E, Haskell A, Elias JA and McDonald DM. Regulated angiogenesis and vascular regression in mice overexpressing vascular endothelial growth factor in airways. Am J Pathol. 2004;165:1071-85.
50. Sano H, Hosokawa K, Kidoya H and Takakura N. Negative regulation of VEGF-induced vascular leakage by blockade of angiotensin II type 1 receptor. Arterioscler Thromb Vasc Biol. 2006;26:2673-80.
51. Waeber C and Walther T. Sphingosine-1-phosphate as a potential target for the treatment of myocardial infarction. Circ J. 2014;78:795-802.
52. Jung K, Kim P, Leuschner F, Gorbatov R, Kim JK, Ueno T, Nahrendorf M and Yun SH.

Endoscopic time-lapse imaging of immune cells in infarcted mouse hearts. Circ Res. 2013;112:891-9.
53. Park Y, Lee J, Kwak JY, Noh K, Yim E, Kim HK, Kim YJ, Broxmeyer HE and Kim JA. Fractalkine induces angiogenic potential in CX3CR1-expressing monocytes. J Leukoc Biol. 2018;103:53-66.
54. Getzin T, Krishnasamy K, Gamrekelashvili J, Kapanadze T, Limbourg A, Hager C, Napp LC, Bauersachs J, Haller H and Limbourg FP. The chemokine receptor CX3CR1 coordinates monocyte recruitment and endothelial regeneration after arterial injury. EMBO Mol Med. 2017.
55. Hughes JE, Srinivasan S, Lynch KR, Proia RL, Ferdek P and Hedrick CC. Sphingosine-1-phosphate induces an antiinflammatory phenotype in macrophages. Circ Res. 2008;102:950-8.
56. Sager HB, Hulsmans M, Lavine KJ, Moreira MB, Heidt T, Courties G, Sun Y, Iwamoto Y, Tricot B, Khan OF, Dahlman JE, Borodovsky A, Fitzgerald K, Anderson DG, Weissleder R, Libby P, Swirski FK and Nahrendorf M. Proliferation and Recruitment Contribute to Myocardial Macrophage Expansion in Chronic Heart Failure. Circ Res. 2016;119:853-64.
57. Wong SP, French JK, Lydon AM, Manda SO, Gao W, Ashton NG and White HD. Relation of left ventricular sphericity to 10-year survival after acute myocardial infarction. Am J Cardiol. 2004;94:1270-5.
58. van den Borne SW, Diez J, Blankesteijn WM, Verjans J, Hofstra L and Narula J. Myocardial remodeling after infarction: the role of myofibroblasts. Nat Rev Cardiol. 2010;7:30-7.
59. Aguero J, Lobo Gonzalez M and Ishikawa K. Route TESI: Main Street for MSC? Circ Res. 2017;120:1055-1056.
60. Meyer GP, Wollert KC, Lotz J, Pirr J, Rager U, Lippolt P, Hahn A, Fichtner S, Schaefer A, Arseniev L, Ganser A and Drexler H. Intracoronary bone marrow cell transfer after myocardial infarction: 5-year follow-up from the randomized-controlled BOOST trial. Eur Heart J. 2009;30:2978-84.
61. Assmus B, Rolf A, Erbs S, Elsasser A, Haberbosch W, Hambrecht R, Tillmanns H, Yu J, Corti R, Mathey DG, Hamm CW, Suselbeck T, Tonn T, Dimmeler S, Dill T, Zeiher AM and Schachinger V. Clinical outcome 2 years after intracoronary administration of bone marrow-derived progenitor cells in acute myocardial infarction. Circ Heart Fail. 2010;3:89-96.
62. Wollert KC, Meyer GP, Lotz J, Ringes-Lichtenberg S, Lippolt P, Breidenbach C, Fichtner S, Korte T, Hornig B, Messinger D, Arseniev L, Hertenstein B, Ganser A and Drexler H. Intracoronary autologous bone-marrow cell transfer after myocardial infarction: the BOOST randomised controlled clinical trial. Lancet. 2004;364:141-8.
63. Schachinger V, Erbs S, Elsasser A, Haberbosch W, Hambrecht R, Holschermann H, Yu J, Corti R, Mathey DG, Hamm CW, Suselbeck T, Assmus B, Tonn T, Dimmeler S and Zeiher AM. Intracoronary bone marrow-derived progenitor cells in acute myocardial infarction. N Engl J Med. 2006;355:1210-21.

Table 1. Quantitative analysis of microvasculature parameters in the cardiac tissue from treated and non-treated mice after myocardial infarction.

	Infarct Untreated	Infarct Treated	Remote Untreated	Remote Treated	Basal
Fractal-Based Metrics					
Fractal Dimension	1.79±0.04	1.78±0.03 ↓	1.86±0.04	1.85±0.04 ↓	1.91±0.01
Lacunarity ($\times10^{-2}$)	96.42±0.84	95.84±1.16 ↓	92.34±0.94	91.46±0.83 ↓*	90.93±0.15
Minkowski-Based Metrics					
Vascular Volume Density (%)	2.62±0.38	2.46±0.26 ↓	3.66±1	3.44±0.8 ↓	3.48±0.21
Vascular Surface Area Density ($\times10^{-3}$) ($\mu m^2/\mu m^3$)	23.79±1.51	24.86±3.13 ↑	41.72±6.31	43.08±5.15 ↑	40.17±1.91
Breadth Density ($\times10^{-3}$)(μm/μm3)	0.97±0.06	1.08±0.23 ↑	2.23±0.31	2.38±0.22 ↑	2.05±0.22
Euler Characteristic Density ($\times10^{-5}$)($1/\mu m^3$)	-1.7±3.09	-1.2±2.87 ↑	1.6±6.89	3.49±9.56 ↑	5.89±1.76
Capillary Volume Density (%)	0.66±0.15	0.76±0.17 ↑	2.31±0.39	2.65±0.31 ↑*	2.36±0.13
Capillary Surface Area Density ($\times10^{-3}$)($\mu m^2/\mu m^3$)	9.94±2.5	11.24±2.75 ↑	32.49±4.57	37.1±2.69 ↑**	32.47±2.08
Enlarged capillary Volume Density (%)	0.58±0.34	0.34±0.21 ↓	0.81±0.63	0.4±0.43 ↓	0.3±0.16
Enlarged capillary Surface Area Density ($\times10^{-3}$)($\mu m^2/\mu m^3$)	4.84±2.55	2.93±1.7 ↓	6.69±5.11	3.47±3.68 ↓	2.51±1.45
SMA+ vessel Volume Density (%)	1.37±0.24	1.35±0.16 ↓	0.53±0.27	0.39±0.26 ↓	0.82±0.1
SMA+ vessel Surface Area Density ($\times10^{-3}$)($\mu m^2/\mu m^3$)	10.21±1.73	11.67±1.67 ↑	4.12±1.78	3.55±2.6 ↓	6.18±0.33
Capillary (%)	26.42±9.74	31.11±7.53 ↑	66.19±15.86	78.94±10.78 ↑*	67.92±3.57
Enlarged capillary (%)	21.05±10.45	13.6±6.98 ↓	19.95±13.19	9.95±8.48 ↓*	8.53±4.54
SMA+ vessel (%)	52.52±6.81	55.29±5.89 ↑	13.86±4.84	11.11±6.6 ↓	23.55±2.56
Graph-Based Metrics					
Vascular segment diameter (μm)	4.23±0.7	3.96±0.6 ↓	3.76±0.62	3.43±0.37 ↓	3.91±0.25
Vascular segment length (μm)	8.58±1.55	8.58±1.4 ↓	9.67±1.23	10.06±1.06 ↑	12.24±1.62
Vascular segment surface (μm^2)	119.08±38.82	112.19±30.08 ↓	121.14±31.15	114.62±18.95 ↓	153.61±26.72
Vascular segment volume (μm^3)	149.58±67.97	132.71±48.83 ↓	135.32±52.18	113.56±27.61 ↓	175.04±37.32
Tortuosity (μm/μm)	1.5±0.06	1.54±0.06 ↑	1.51±0.08	1.54±0.06 ↑	1.47±0.01
SMA+ & Pdgfrb related metrics					
Myofibroblasts abundance	0.5±0.06	0.43±0.09 ↓*	0.04±0.03	0.03±0.02 ↓	0.02±0.01
Vessels covered with Pdgfrb (%)	76.95±8.09	76.59±11.75 ↓	87.07±7.1	87.21±5.71 ↑	88.75±2.85
Vessels covered with SMA (%)	38.19±4.82	40.98±5.7 ↑	15.98±6.07	12.26±6.01 ↓	24.18±3.27
SMA+ layer thickness (μm)	3.72±0.82	3.68±0.51 ↓	3.85±0.39	3.7±0.79 ↓	4.5±0.52
SMA+ perivascular cells [a]	16.19±3.65	18.33±4.39 ↑	6.1±2.78	4.93±2.56 ↓	8.33±0.66
Efficiency in oxygen diffusion					
Median Extravascular Distance (μm)	13.38±1.52	11.76±2.21 ↓	5.68±0.51	5.34±0.28 ↓	5.63±0.35
Maximal Extravascular Distance (μm)	43.63±7.04	36.02±8.59 ↓*	12.53±1.2	11.69±0.76 ↓	13.19±1
Additional cell-related metrics					
Endothelial cells ($\times10^5$) [b]	26.71±2.37	30.31±4.28 ↑*	35.43±5.83	39.79±6.04 ↑	31.63±4.75

[a] Number per mm vascular length
[b] Number per mm3 vascular volume

Mean±standard deviation of all parameters for cardiac tissue from treated (BM^{hVEGF}+BM^{hSPHK1}) and non-treated (PBS) mice along with pairwise comparisons among the different tissue conditions. Capillaries correspond to CD31+ & SMA- vessels of diameter < 5 μm, enlarged capillaries to CD31+ & SMA- vessels of diameter ≥ 5 μm, and SMA+ vessels to CD31+ & SMA+ vessels regardless their diameter. Up-arrows and down-arrows indicate increase and decrease respectively of the parameter value for (i) tissue from infarcted areas of subjects treated with BM^{hVEGF}+BM^{hSPHK1} compared with tissue from infarcted areas of untreated subjects, and (ii) tissue from remote areas of subjects treated with BM^{hVEGF}+BM^{hSPHK1} compared to tissue from remote areas of untreated subjects. Red (for increase) and blue (for decrease) colors are used to denote that the difference is statistically significant. *, and ** represent p-value< 0.05, and 0.01 respectively. The p-values were calculated by means of two-sample t-test.

Figure legends

Figure 1. **Sequential BM cell delivery of VEGF and S1P increases capillary volume density and endothelial cell number on the infarcted heart post-MI**. **A**. Left panels: representative maximal intensity projections from confocal microscopy images of transverse sections of mouse hearts stained for endothelial cells (CD31, gray) and smooth muscle cells (SMA, red). Right panels: bar graphs showing total vascular volume density and the number of endothelial cells per vascular volume in the infarct zone of treated and non-treated mice 28 days post-I/R. Scale bar, 50 μm. **B**. Representative images of segmented vessels in three categories: capillaries ($CD31^+SMA^-$ < 5 μm diameter, red), enlarged capillaries ($CD31^+SMA^-$ > 5.1 μm diameter, yellow), and arterioles/SMA+ vessels ($CD31^+SMA^+$, white) in the infarct zone of treated and non-treated hearts; scale bar 50μm. **C**. Bar graphs showing volume densities for the three-vessel categories as well as percentage representation of each vessel type out of the total vasculature. **D-F.** Representative images and bar graphs as described in A-C corresponding to the remote zone of hearts from treated and non-treated mice 28. Data are represented as mean ± SD of n=9 and n=12 mice for non-treated and treated groups respectively analyzed in 2 independent experiments. Parametric t-test was used for statistical comparison. *, $p<0.05$, **, $p<0.01$, ***, $p<0.001$.

Figure 2. **BM cell sequential delivery of VEGF and S1P reduces intercapillary distances in the post-infarcted heart**. **A**. Representative images of extravascular distance maps from the infarct and remote zone of treated and control mice 28 days post-MI. **B**. Bar graphs show the quantification of maximal extravascular distances in the conditions shown in A. Data are represented as mean ± SD of n=9 and n=12 mice for non-treated and treated groups respectively analyzed in 2 independent experiments. Parametric t-test was used for statistical comparison. *, $p<0.05$, **, $p<0.01$, ***, $p<0.001$.

Figure 3. Sequential BM cell-secreted VEGF and S1P angiotherapy reduces myofibroblast abundance and collagen fiber compaction in the infarcted heart post-I/R. **A**. Representative images from Masson-Trichrome-stained transverse sections of hearts from treated and control groups 28 days post-I/R. **B.** Graphs shows percentage of left ventricle area covered by scar tissue in serial cuts spanning the whole-heart from the apex (1) to the base (7). **C.** Bar graph shows the percentage of left ventricle scar area in the transverse section of the base of the heart (closest to the valves). **D**. Pseudo-colored representation of confocal microscopy images of transverse sections from the infarct zone of treated and control hearts stained for CD31 and PDGFRβ in which vessels ($CD31^+$) are shown in red, perivascular cells ($PDGFR\beta^+$ cells touching vessels) in blue and myofibroblasts ($PDGFR\beta^+$ cells distant from the vessels) in green. **E**. Bar graphs represent myofibroblast abundance in the infarct and remote zones. **F**. Representative images of collagen fibers obtained by second harmonic generation (SHG) multiphoton microscopy in transverse sections of hearts from treated and control groups 28 days post-I/R. **G.** Bar graphs show the quantitation of the first order parameters skewness (asymmetry of pixel distribution) and kurtosis (gray-tone spread-out distribution) in SHG images. Data are represented as mean ± SD. n=11 and 16 (**B**, **C**), n=9 and 12 (**D, E**), and n=9 and 10 (**F, G**) mice of non-treated and treated groups respectively analyzed in 3 (**B**, **C**) and in 2 (**D-G**) independent experiments. Data were statistically compared by two-way ANOVA (**B**), parametric t-test (**C**), and nonparametric Mann-Whitney U test (**D-G**). *, $p<0.05$, **, $p<0.01$, ***, $p<0.001$.

Figure 4. Sequential delivery of VEGF and S1P by LV-transduced BM cells limits adverse cardiac remodeling post-MI. **A.** Graphs show the left ventricle end-systolic (LVESV) and end-diastolic (LVEDV) volumes of hearts from basal (no I/R), and from control (PBS) or VEGF/S1P-treated mice at 3 and 28 days post-I/R. **B**. Graph shows the left ventricle posterior wall end-diastolic thickness calculated in M-mode ultrasound images in hearts from control (PBS) or VEGF/S1P-treated mice at 28 days post-I/R. **C**. Bar graphs show the heart roundness

coefficient quantitated in macroscopic images from hearts of treated and non-treated mice 28 days post-I/R. **D**. Maximal intensity projections from confocal microscopy images of the remote area from pan-laminin (green)-stained transverse sections of hearts from treated and non-treated mice 28 days post-I/R. Scale bar, 50 μm. **E**. Bar graphs shows the quantification of cardiomyocyte area and perimeter from pan-laminin-stained images (D). **F**. Representative western blots for Col1a1 and Atp2a2 protein expression in hearts from treated and non-treated mice 28 days post I/R (top) and graphs with the quantification expressed as fold change (F.C., bottom). Tubulin is included as loading control. n=6 mice from non-treated (PBS) and treated (BM^{hVEGF}+BM^{hSPHK1} groups. Data are shown as mean ± S.E.M. and were statistically compared with parametric t-test; *$p<0.05$. **G**. Representative maximal intensity projections from confocal microscopy images of heart sections from treated and non-treated mice 28 days post-I/R stained for cardiomyocytes (α-actinin, gray) and Atp1a2 (red). Yellow squares indicate the magnified areas. Scale bar, 100 μm and 50 μm in the magnified views. Data are represented as mean ± SD. n=6 mice for non-I/R and n=11-12 and 16-18 mice for non-treated and treated groups respectively analyzed in 3 independent experiments (**A-E**). n=6 mice for non-treated and treated groups respectively analyzed in 2 independent experiments (**F**). Data were statistically compared with one-way ANOVA (**A**) and parametric t-test (**B-F**). *, $p<0.05$, **, $p<0.01$, ***, $p<0.001$.

Figure S1. **Pro-angiogenic efficacy of combined VEGF and S1P in mouse aortic rings**. **A**. Maximal intensity projections from confocal microscopy images of mouse aortic rings stained for IB4 (green) and αSMA (red) 7 days after the indicated treatments. Scale bar, 200 μm. **B**. Bar graph shows the $IB4^+$ volume covered by the sprouts. **C**. Bar graph shows the percentages of endothelial sprout volume covered or not-covered by SMA^+ cells. Data are represented as mean ± SD.n=18±2 rings per group in two independent experiments. Data were statistically compared with nonparametric Kruskal-Wallis test *, $p<0.05$, **, $p<0.01$, ***, $p<0.001$.

Figure S2. Expression and secretion of VEGF and S1P by LV-transduced HEK and mouse bone marrow (BM) cells. A. Schematic of the provirus showing the genes of interest inserted downstream to the SFFV promoter. **B.** Graph shows the relative *VEGFA* and *SPHK1* mRNA levels quantified by qPCR in untransduced or transduced HEK cells; note that Ct values are inverse to mRNA levels. **C, F.** Graph shows the amount of secreted hVEGFA measured by ELISA in supernatants from LV_hVEGFA-transduced and non-transduced HEK (**C**) and bone marrow cells (**F**). **D, G.** Graph shows the relative abundance of S1P in cell lysates from LV_hSPHK1-transduced and non-transduced HEK (**D**) and bone marrow (**G**) cells analyzed by mass spectrometry. **E.** Graph shows the percentage of GFP^+ BM cells at 1, 3 and 6 days after LV_GFP transduction at the indicated multiplicity of infection (MOI). Data are represented as mean values ± SD. qPCR n=3 technical replicates; ELISA n=6-7 technical replicates from four experiments for HEK and BM cells; S1P measurement n=3 with 3 technical replicates in one experiment. Data were statistically compared with parametric t-test. $p<0.05$, **, $p<0.01$, ***, $p<0.001$.

Figure S3. **Mouse BM cells home to the infarcted heart tissue and their LV-transduction increases monocyte CX_3CR1 expression**. **A**. Representative confocal microscopy images of heart sections obtained 4 days post-I/R and stained with anti-RFP (red) and Hoechst (blue, nuclei) 24h after i.v. injection of dtTomato_BM cells; bottom right panels show magnified views. Auto-fluorescence of myocardium is shown in green channel. Scale bar 50μm and 10μm in the magnified view. **B and C**. Representative flow

cytometry plots show untransduced (in B) and transduced (in C) BM cells stained with the indicated antibodies. **D-F**. Bar graphs show the percentage of neutrophils ($CD11b^{+}F4/80^{-}Ly6C^{mid}SSC^{hi}$), macrophages ($CD11b^{hi}F4/80^{+)}$, and myeloid progenitors ($CD11b^{+}F4/80^{-}Ly6C^{low}$). **G**. Bar graphs show the percentage of monocytes ($CD11b^{hi}F4/80^{-}Ly6C^{hi}$; left), and their expression of CX_3CR1 (middle) and CCR2 (right) receptors represented as median fluorescence intensity (MFI). Data are represented as mean ± SD; n=3. Data were statistically compared with one-way ANOVA test. $p<0.05$, **, $p<0.01$, ***, $p<0.001$.

Figure S4. Strategy for sequential delivery of VEGF/S1P by LV-transduced BM cells after MI in vivo and effect in vitro on aortic ring assays. A. The scheme depicts the experimental designs for sequential delivery of VEGF and S1P by LV-transduced BM cells injected i.v. at days 4 and 7 post-I/R in mice and the analysis performed. **B**. Maximal intensity projections from confocal microscopy images of mouse aortic rings stained for CD31 (gray) and αSMA (red) 7 days after the indicated culture with bone marrow (BM) cells are shown to the left. Scale bar, 200 μm. To the right, bar graphs show the $CD31^{+}$ vascular area covered by the sprouts (top) and the percentage of $CD31^{+}$ vascular sprout area covered or not-covered by SMA^{+} cells (bottom). Data are represented as mean ± SD, n=25±2 rings per group in 3 independent experiments. Data were statitically compared with Kruskal-Wallis test. *, $p<0.05$, **, $p<0.01$, ***, $p<0.001$.

Figure S5. Sequential VEGF/S1P gene-cell therapy does not impact on cardiac contractility post-MI. A. Representative maximal intensity projections from confocal microscopy images of heart sections obtained 28 days post-I/R from mice non-treated or treated with the combined angiotherapy and stained for cardiomyocytes (α-actinin, gray) and apoptosis (cleaved caspase-3, red). Yellow squares indicate the magnified area. Scale bar, 100 μm and 50 μm in the magnified views. **B**. Representative images of ultrasound transverse analysis (M-mode) is shown from hearts of mice non-treated or treated with the

combined angiotherapy 28 days post-I/R. **C**. Graphs show the left ventricle ejection fraction (LVEF) and stroke volume (SV) of basal mice (no I/R) and of control (PBS) and VEGF/S1P-treated mice 3 and 28 days post-I/R. Data are represented as mean ± SD. n=6-11 mice for non-I/R and n=11-12 and 16-18 mice for non-treated and treated groups respectively analyzed in 3 independent experiments. Data were statistically compared with one-way ANOVA test. *, $p<0.05$, **, $p<0.01$, ***, $p<0.001$.

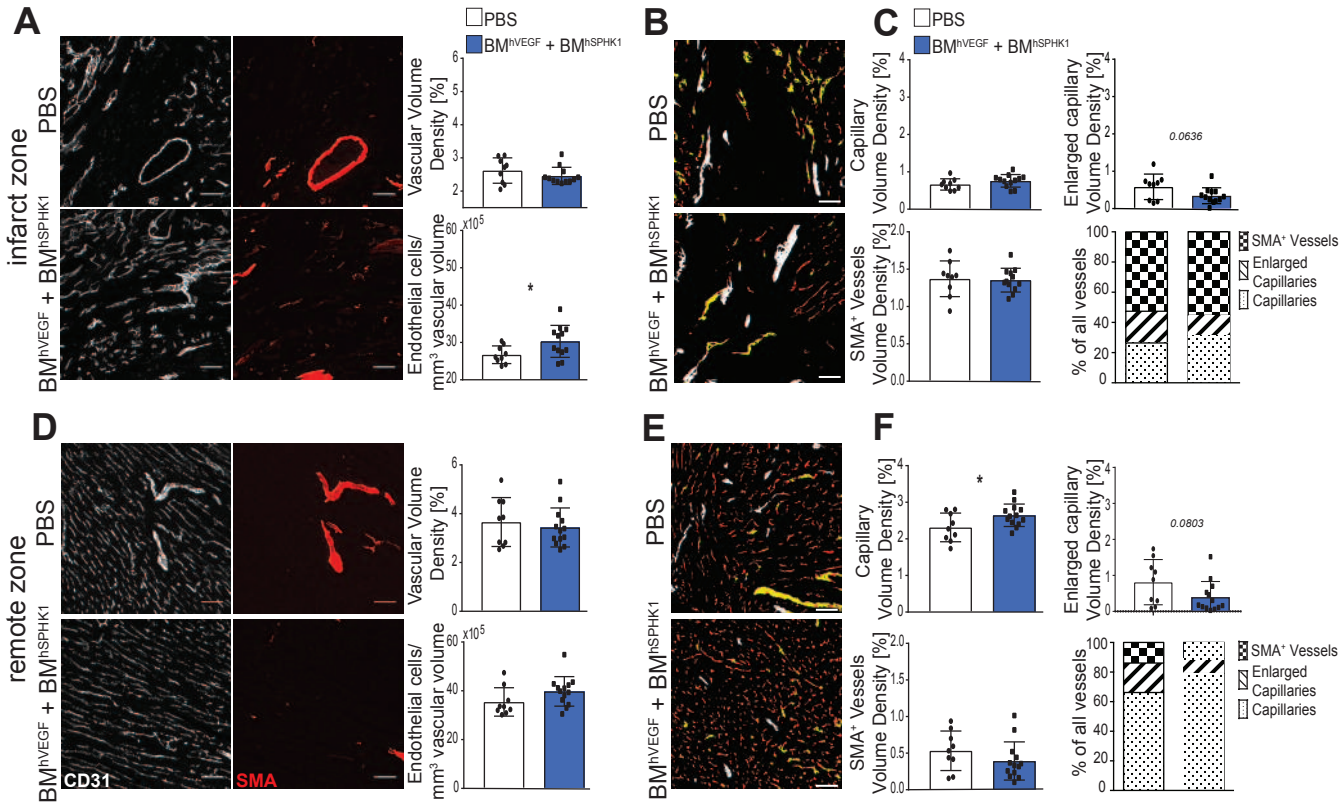
A
B
C
D
E
F
infarct zone
remote zone
PBS
BM^hVEGF + BM^hSPHK1
CD31
SMA
Vascular Volume Density [%]
Endothelial cells/ mm³ vascular volume
x10^5
Capillary Volume Density [%]
SMA⁺ Vessels Volume Density [%]
Enlarged capillary Volume Density [%]
0.0636
0.0803
% of all vessels
SMA⁺ Vessels
Enlarged Capillaries
Capillaries
*

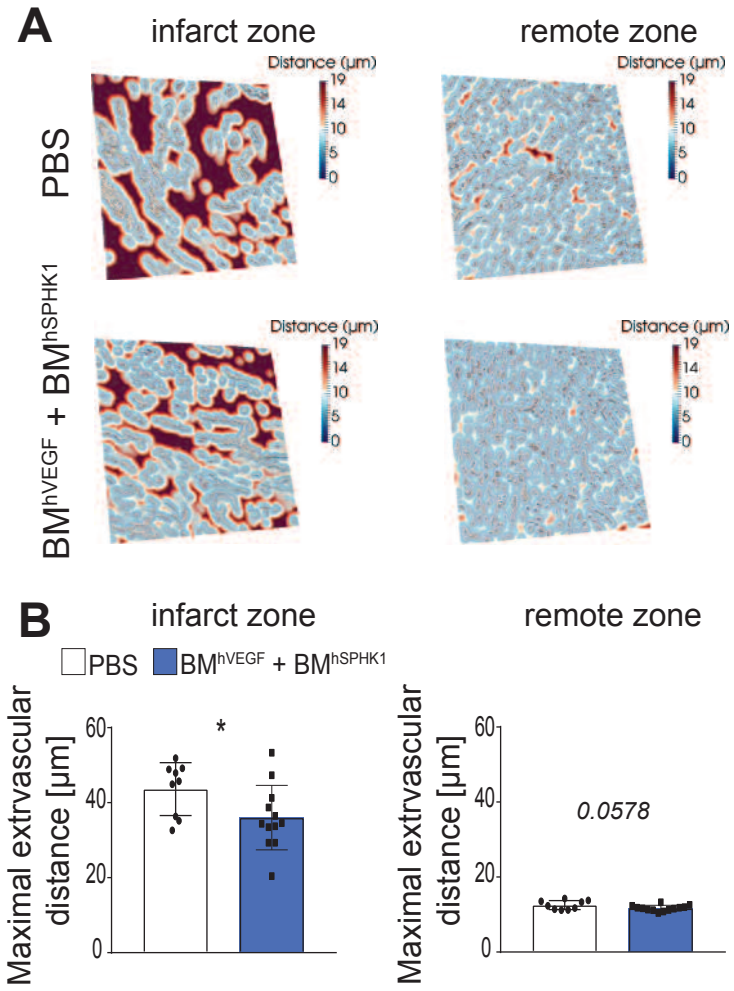
A
infarct zone
remote zone
PBS
BMhVEGF + BMhSPHK1
Distance (µm)
19
14
10
5
0
B
infarct zone
remote zone
PBS
BMhVEGF + BMhSPHK1
Maximal extrvascular distance [µm]
60
40
20
0
*
0.0578

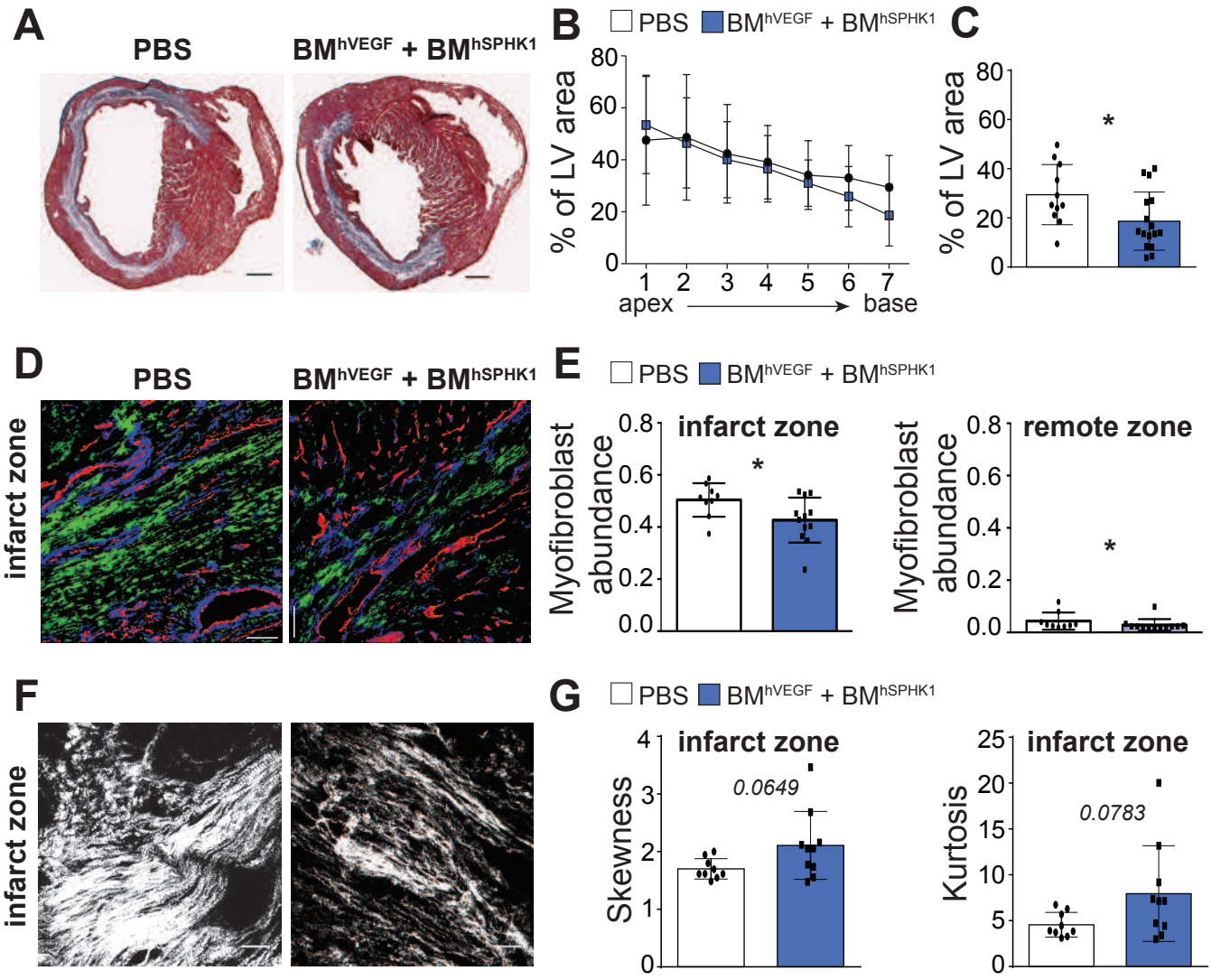
A
PBS
BM^hVEGF + BM^hSPHK1
B
PBS
BM^hVEGF + BM^hSPHK1
% of LV area
apex
base
C
% of LV area
*
D
PBS
BM^hVEGF + BM^hSPHK1
infarct zone
E
PBS
BM^hVEGF + BM^hSPHK1
Myofibroblast abundance
infarct zone
remote zone
*
F
infarct zone
G
PBS
BM^hVEGF + BM^hSPHK1
Skewness
infarct zone
0.0649
Kurtosis
infarct zone
0.0783

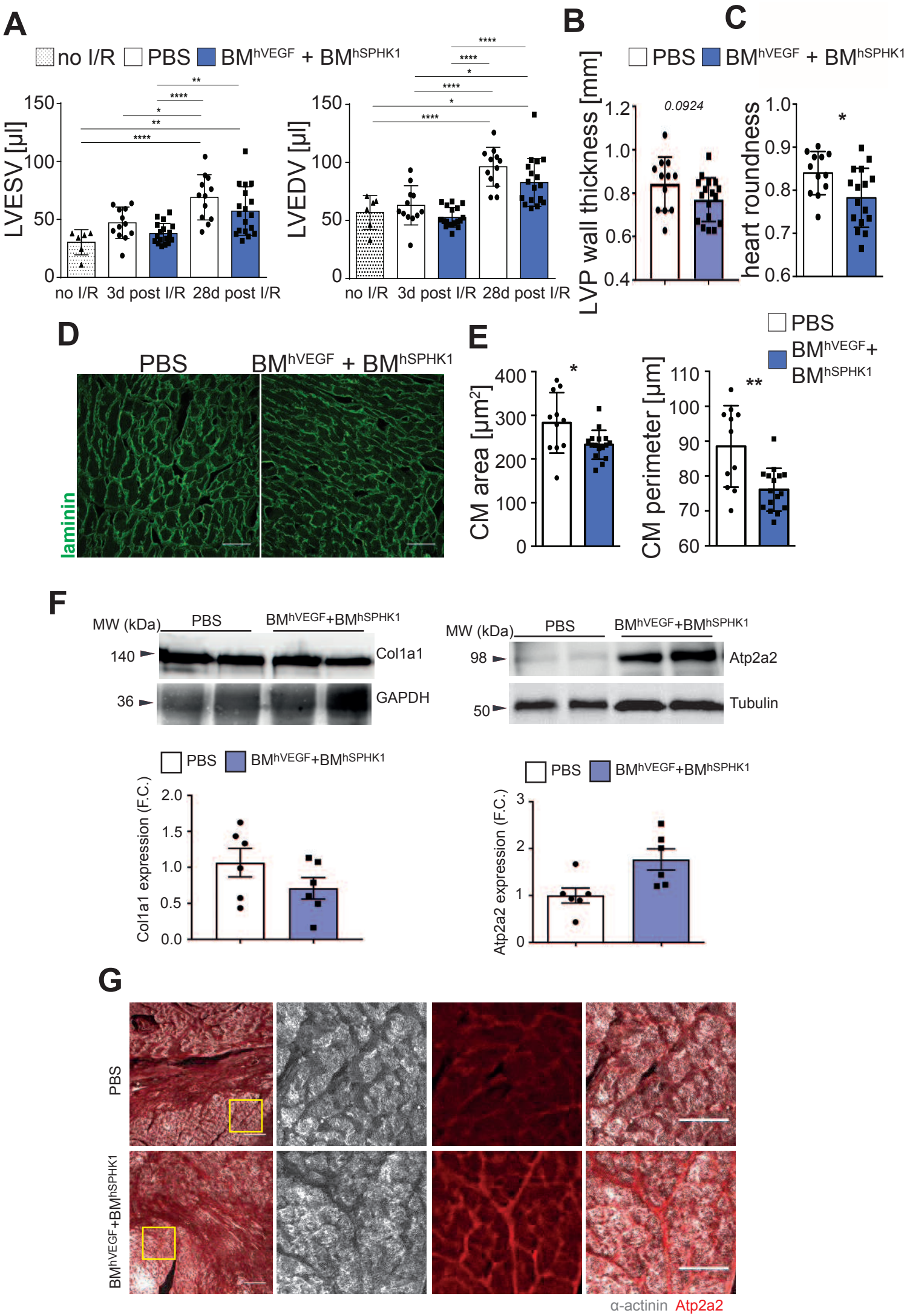
A
no I/R
PBS
BM^hVEGF + BM^hSPHK1
LVESV [µl]
LVEDV [µl]
no I/R
3d post I/R
28d post I/R
B
LVP wall thickness [mm]
0.0924
C
heart roundness
D
PBS
BM^hVEGF + BM^hSPHK1
laminin
E
CM area [µm²]
CM perimeter [µm]
F
MW (kDa)
Col1a1
GAPDH
Atp2a2
Tubulin
Col1a1 expression (F.C.)
Atp2a2 expression (F.C.)
G
α-actinin Atp2a2

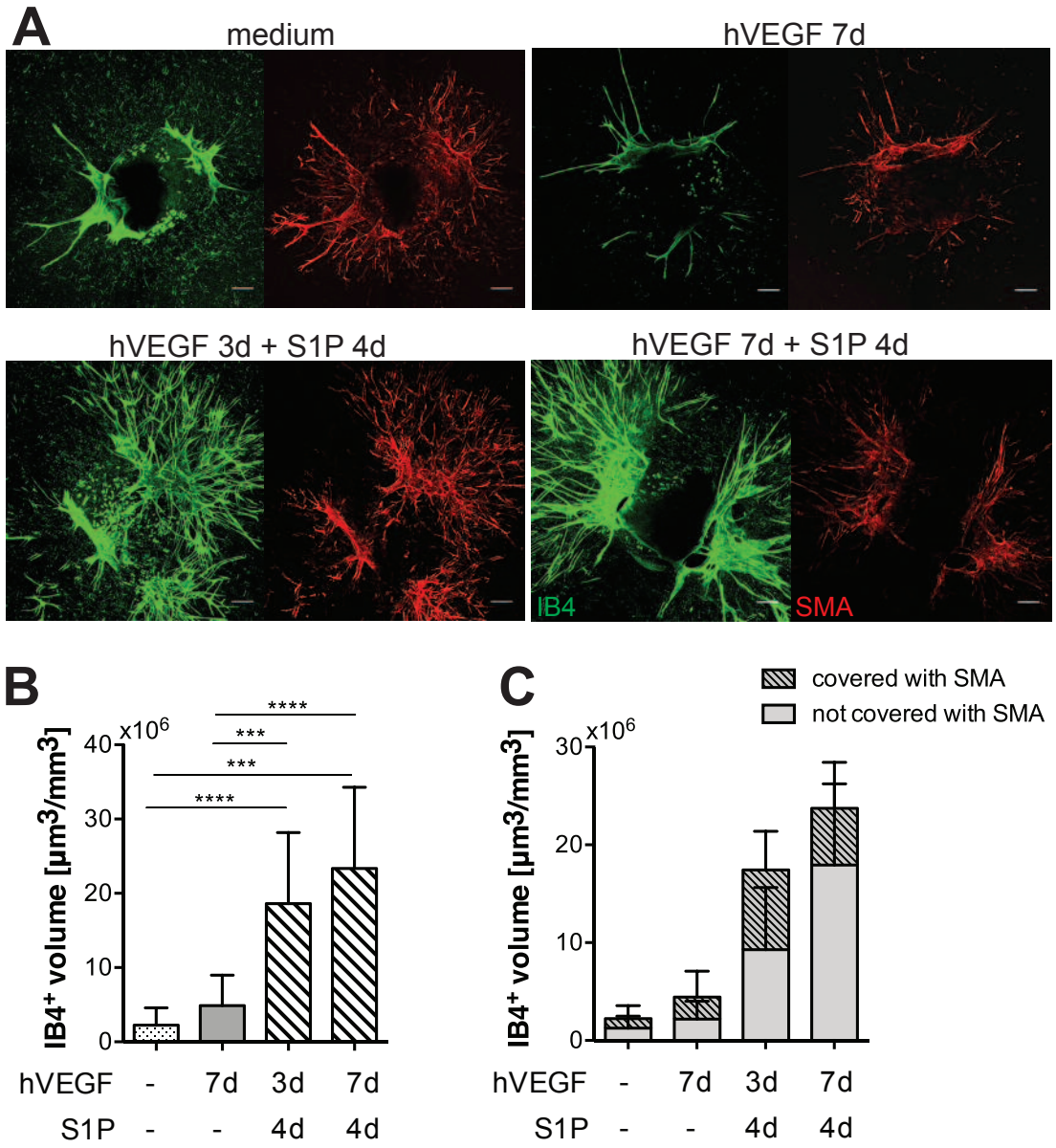
A
medium
hVEGF 7d
hVEGF 3d + S1P 4d
hVEGF 7d + S1P 4d
IB4
SMA
B
x10^6
IB4+ volume [µm3/mm3]
40
30
20
10
0
****
***
***
****
hVEGF - 7d 3d 7d
S1P - - 4d 4d
C
covered with SMA
not covered with SMA
x10^6
IB4+ volume [µm3/mm3]
30
20
10
0
hVEGF - 7d 3d 7d
S1P - - 4d 4d

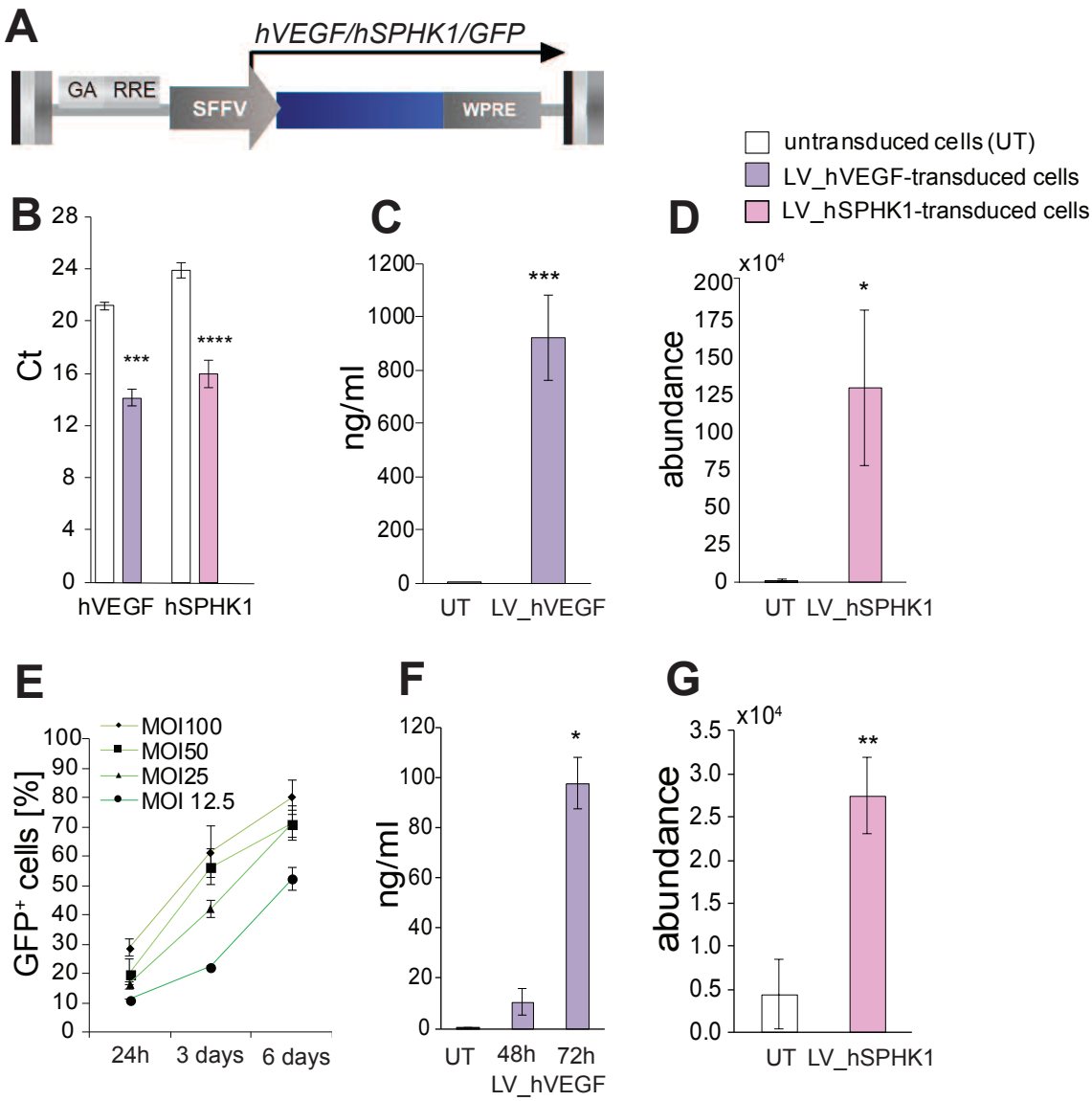
A
hVEGF/hSPHK1/GFP
GA
RRE
SFFV
WPRE
untransduced cells (UT)
LV_hVEGF-transduced cells
LV_hSPHK1-transduced cells
B
Ct
28
24
20
16
12
8
4
0
***
****
hVEGF
hSPHK1
C
ng/ml
1200
1000
800
600
400
200
0
***
UT
LV_hVEGF
D
x10⁴
abundance
200
175
150
125
100
75
50
25
0
*
UT
LV_hSPHK1
E
GFP⁺ cells [%]
MOI100
MOI50
MOI25
MOI 12.5
100
90
80
70
60
50
40
30
20
10
0
24h
3 days
6 days
F
ng/ml
120
100
80
60
40
20
0
*
UT
48h
72h
LV_hVEGF
G
x10⁴
abundance
3.5
3.0
2.5
2.0
1.5
1.0
0.5
0.0
**
UT
LV_hSPHK1

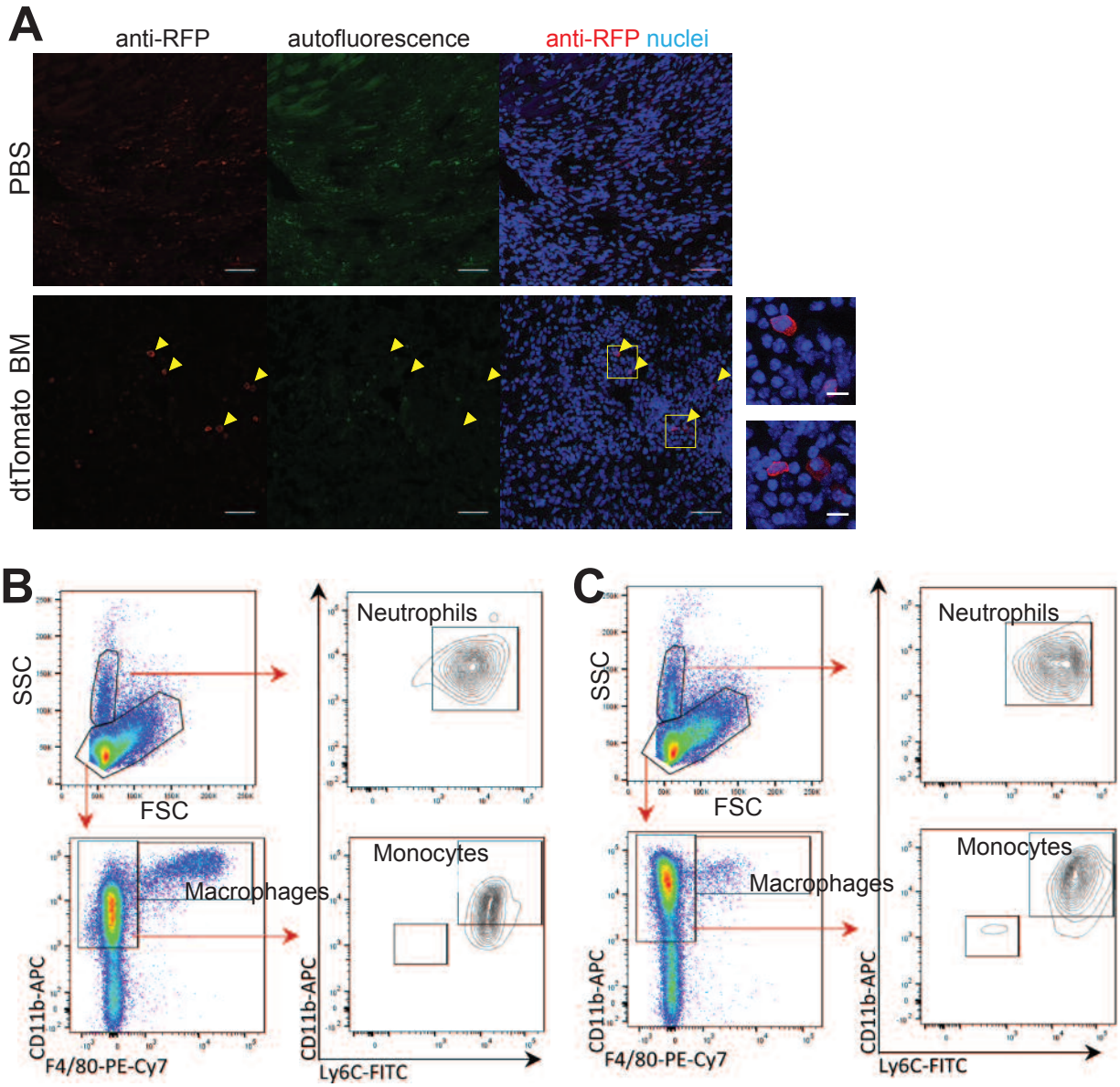
A
anti-RFP
autofluorescence
anti-RFP nuclei
PBS
dtTomato BM
B
SSC
FSC
Neutrophils
Monocytes
Macrophages
CD11b-APC
F4/80-PE-Cy7
Ly6C-FITC
C
SSC
FSC
Neutrophils
Monocytes
Macrophages
CD11b-APC
F4/80-PE-Cy7
Ly6C-FITC

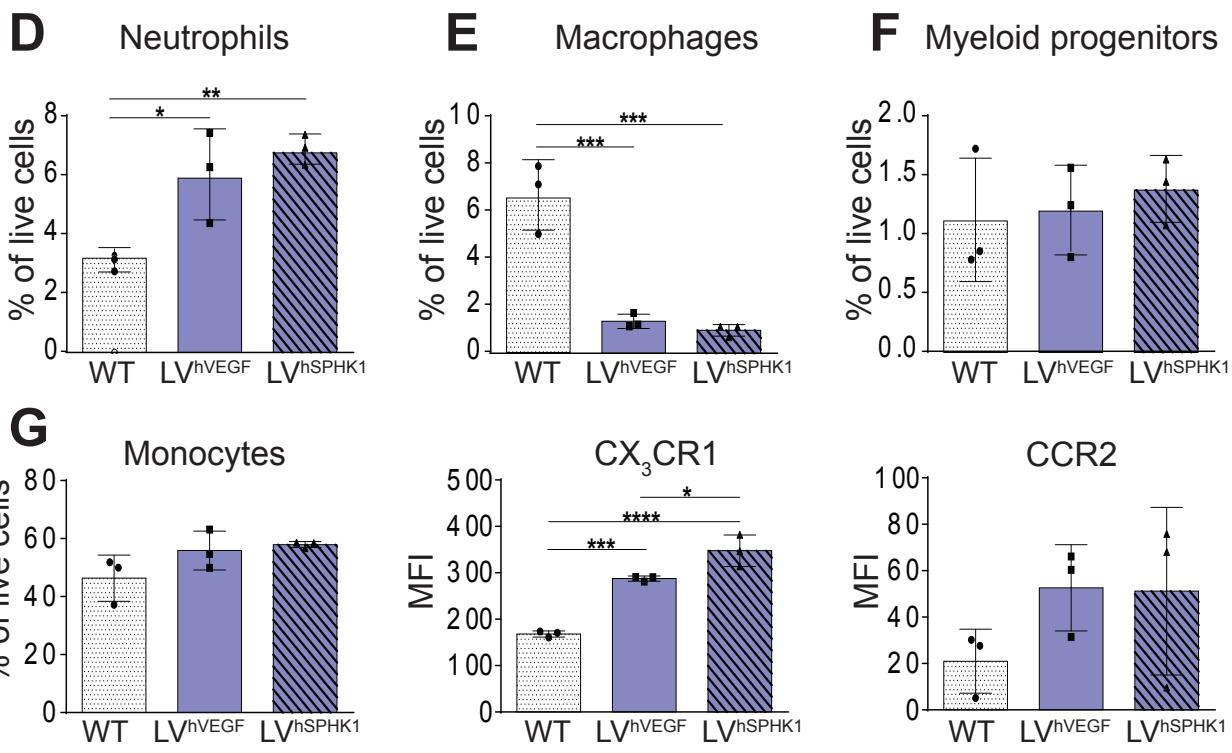
D
Neutrophils
% of live cells
WT
LVhVEGF
LVhSPHK1
E
Macrophages
% of live cells
WT
LVhVEGF
LVhSPHK1
F
Myeloid progenitors
% of live cells
WT
LVhVEGF
LVhSPHK1

G
Monocytes
% of live cells
WT
LVhVEGF
LVhSPHK1
CX3CR1
MFI
WT
LVhVEGF
LVhSPHK1
CCR2
MFI
WT
LVhVEGF
LVhSPHK1

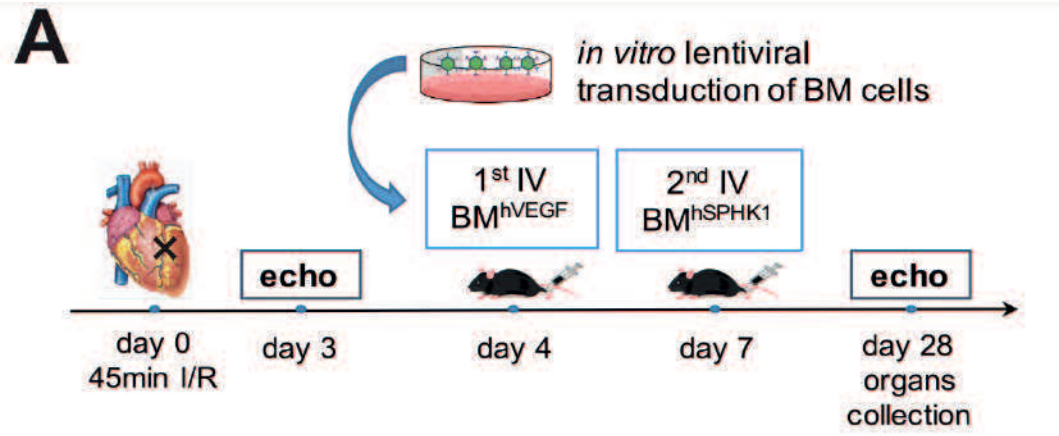
A
in vitro lentiviral transduction of BM cells
1st IV BMhVEGF
2nd IV BMhSPHK1
echo
echo
day 0 45min I/R
day 3
day 4
day 7
day 28 organs collection

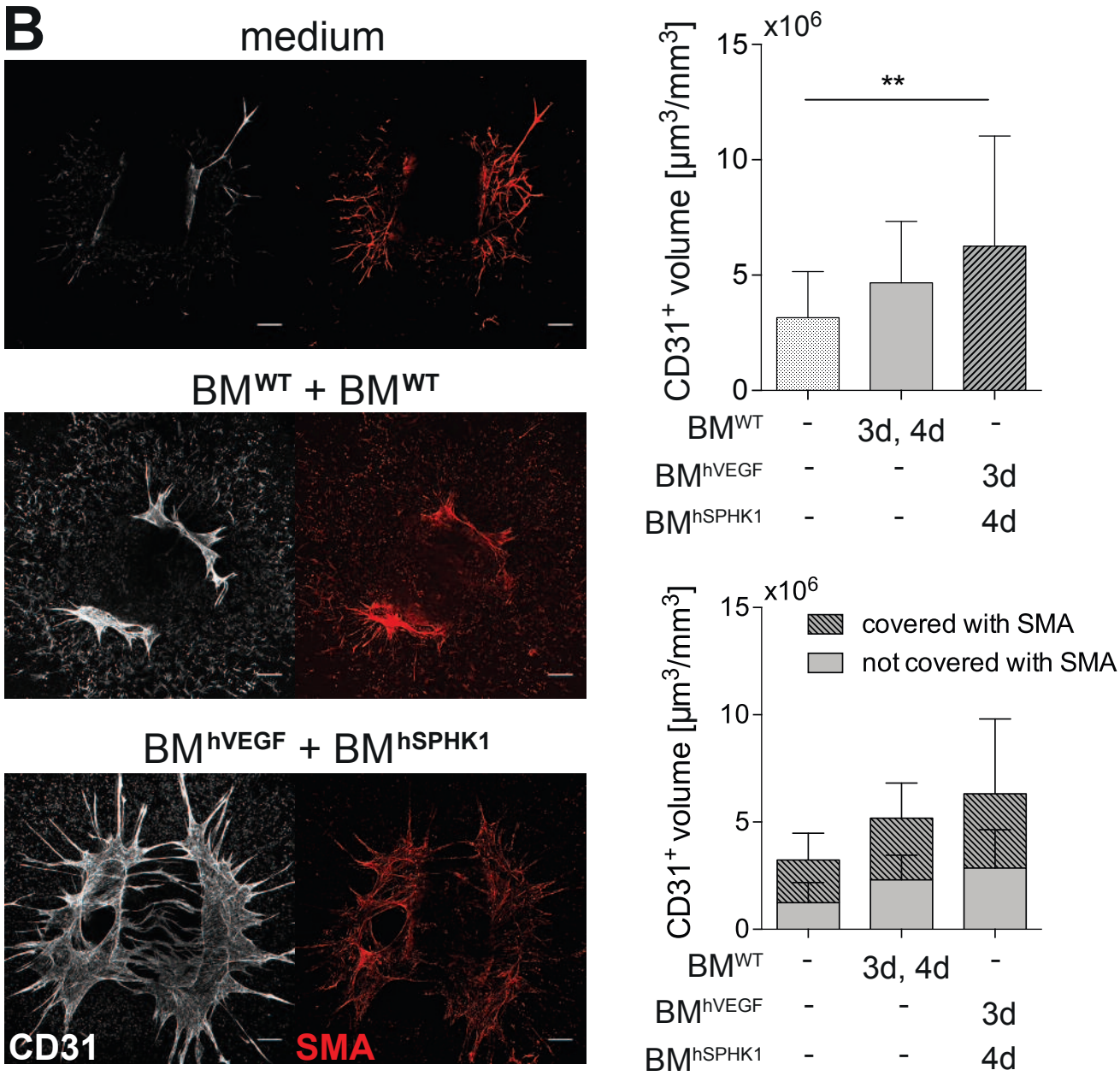
B
medium
BMWT + BMWT
BMhVEGF + BMhSPHK1
CD31
SMA
x10^6
CD31+ volume [µm3/mm3]
15
10
5
0
**
BMWT - 3d, 4d -
BMhVEGF - - 3d
BMhSPHK1 - - 4d
covered with SMA
not covered with SMA

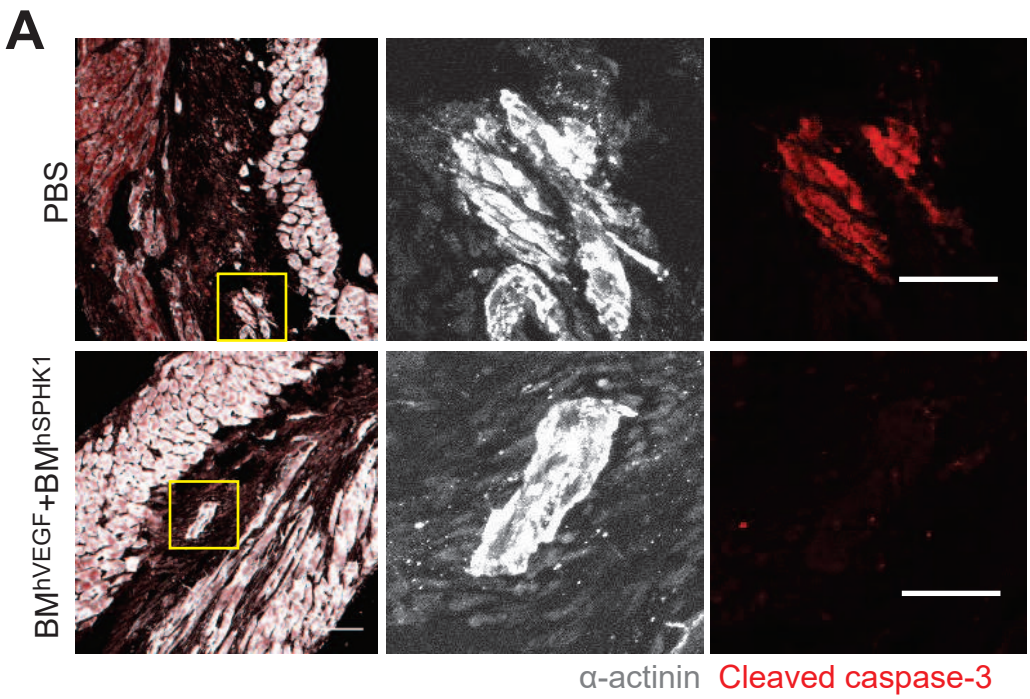
A
PBS
BMhVEGF+BMhSPHK1
α-actinin
Cleaved caspase-3

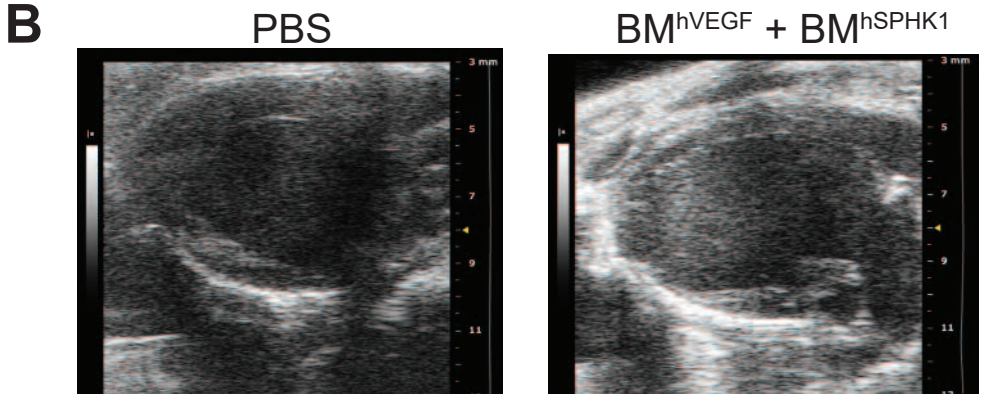
B
PBS
BMhVEGF + BMhSPHK1

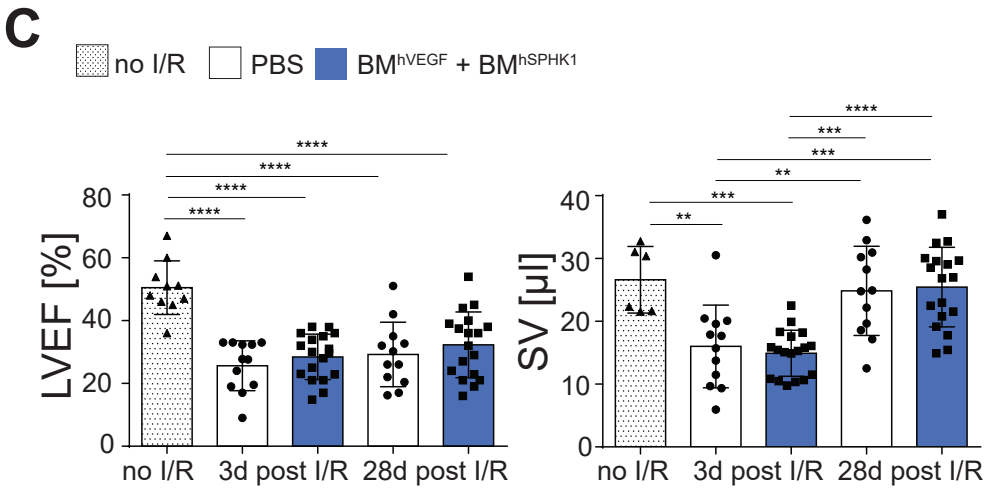
C
no I/R
PBS
BMhVEGF + BMhSPHK1
LVEF [%]
SV [µl]
no I/R
3d post I/R
28d post I/R

Supplemental Methods and Materials

Lentiviral vector (LV) construction and production

VEGFA, *ANG1*, *SPHK1* and *GFP* cDNAs were amplified by PCR using primers containing AgeI and SalI restriction sites (see below). Amplified cDNAs were then inserted downstream to the SFFV promoter of an SFFV.insert.WPRE LV described in[1]. Designed primers are summarized in Table 1. Resulting LVs expressing *VEGFA*, *SPHK1* and GFP were named LV_hVEGF, LV_SPHK1 and LV_GFP accordingly.

Table 1. Primers designed for LV cloning.

Gene	Primer	Sequence
hVEGF-A	Fwd	5'-AAAAAACCGGTGCCGCCATGAACTTTCTGCTGTCTTGG-3'
	Rev	5'-AAAAAGTCGACCTGTCGATGGTGATGGTGT-3'
hSPHK1	Fwd	5'-AAAAAACCGGTGCCGCCATGTCCGCTCAAGTTCTGG-3'
	Rev	5'-AAAAAGTCGACTCATAAGGGCTCTTCTGGCGGT-3'
GFP	Fwd	5'-AAAGTCGACCAGTTAGCCTCCCCCATCTC-3'
	Rev	5'-AAAACCGGTATCCACGCTGTTTTGACCT-3'

Quantitative PCR

HEK cells were transduced with cell supernatants containing non-concentrated LV particles. Transduced HEK cells were then kept in culture for a few passages. Subsequently, the cells were harvested and total RNA isolation was performed using the RNeasy Mini or Micro kit (QIAGEN), depending on the amount of cells. A reverse transcription reaction of 1μg of RNA was performed using the MultiScribe reverse transcriptase (High-Capacity cDNA Reverse Transcription Kit, Applied Biosystems) according to the manufacturer's protocol, with the addition of an RNAse inhibitor (RNasin, Promega). A qPCR reaction was performed in the ABI PRISM® 7900HT FAST Real-Time PCR System using the SYBR®Green dye. Experiments were carried out using three housekeeping genes *hHPRT*, *hGAPDH* and *hYWHAZ*. All experiments included H_2O sample as a template control, as well as non-transduced cells as a negative control. Primers are summarized in Table 2.

Table 2. Primers used for qPCR analysis

Gene	Primer	Sequence
VEGFA	Fwd	5'-CTACCTCCACCATGCCAAGT-3'
	Rev	5'-CTCGATTGGATGGCAGTAGC-3'
SPHK1[1]	Fwd	5'-CATTATGCTGGCTATGAGCAG-3'
	Rev	5'-GTCCACATCAGCAATGAAGC-3'
GAPDH	Fwd	5'-GGAGCGAGATCCCTCCAAAAT-3'
	Rev	5'-GGCTGTTGTCATACTTCTCATGG-3'
HPRT	Fwd	5'-CCTGGCGTCGTGATTAGTGAT-3'
	Rev	5'-AGACGTTCAGTCCTGTCCATAA-3'
YWHAZ	Fwd	5'-CCTGCATGAAGTCTGTAACTGAG-3'
	Rev	5'-GACCTACGGGCTCCTACAACA-3'

[1]*sequence described in*[2]

ELISA

To detect the presence of VEGFA in the cell supernatants, an R&D ELISA kit was used (DVE00). Transduced HEK cells, as well as an untransduced control, were seeded on a 24-well plate in 0.5ml of OPTI-MEM medium (Gibco) with 1% FBS, 100U/ml penicillin, 100U/ml streptomycin. After approximately 30h incubation, supernatants were collected and kept in -20°C. BM cells were incubated overnight with LVs at MOI 50. After washing the virus, cells were seeded in a non-adherent 6-well plate at a density of $2x10^6$/ml and the first collection of supernatant was performed 48h after adding the virus. Next, cells were seeded back in culture and second supernatants were harvested 72h after adding the virus and stored at -20°C. ELISA kit for VEGFA was performed in proper dilutions according to the manufacturer's instruction. Non-transduced cells of both types served as a negative control and medium correction was performed using medium corresponding to each cell types. Optical density was determined using the Benchmark Plus microplate spectrophotometer (BIO-RAD) set at 450nm with wavelength correction at 540nm. Standard curves were created using CurveExpert software.

Quantitative assessment of S1P by mass spectrometry

In order to assess the presence of S1P three technical replicates were analyzed from LV_hSPHK1-transduced and non-transduced HEK and BM cells. The cell pellets (1×10^6 counts each) were thaw on ice and subjected to three freeze–thaw cycles for complete cell disruption, protein precipitation and metabolite extraction. Briefly, samples were suspended in 100µL mixture composed by Methanol:Ethanol (1:1 v/v), vortex-mixed, placed in liquid nitrogen for 10s and thaw in an ice bath (for 10s) three times. Samples were then sonicated for 6 min and vortex-mixed for 1 min. The entire protocol was repeated 3 times. Subsequently samples were centrifuge at 18000 *g* for 20 min at 10°C and the supernatants were collected and dried-out in Speedvac (Savant SPD131DDA concentrator, Savant RVT5105 refrigerated vapor trap and OFP400 vacuum pump, ThermoFisher Scientific, Waltham, Massachusetts, USA) for 2 hours at room temperature. High-resolution parallel reaction monitoring (PRM) of S1P were carried-out on a Ultimate 3000 UHPLC focused system (ThermoFisher Scientific) coupled to an Elite Orbitrap Hybrid Ion Trap-Orbitrap Mass Spectrometer (ThermoFisher Scientific), operating in positive full scan mode from 70 to 1000 m/z at 60000 resolution. Sample were resuspend in 50 µL of a mixture composed of ACN:H2O (10:90, v:v) and 10 µL were injected onto an Agilent mRP-Recovery C18 column (100 ×0.5 mm, 5 µm) which was thermostated at 55°C. S1P was eluted at 100 µL/min with solvent A composed of water with 0.1% formic acid, and solvent B composed of acetonitrile with 0.1% formic acid. The gradient started from 5% to 95% of B in 20 min, keeping constant for 6 min and returned to starting conditions in 0.2 min, finally by keeping the re-equilibration at 90% of B for 8.8 min. Finally, abundance values of S1P peak area were obtained using the Qual Browser software (version 4.0, Thermo scientific).

Aortic rings assay

To assess the angiogenic response for various stimuli in vitro, the aortic rings assay described in[3] was used. Briefly, aortas were dissected from 7-10 week old BL6 male mice, cleaned from fat tissue, and cut into approximately 1mm pieces. After overnight starvation in OPTI-MEM (Gibco), 2mM L-glutamine, 100U/ml penicillin, 100U/ml streptomycin medium, rings were embedded in 1mg/ml rat tail Collagen type I (Merck Millipore) matrix in a 96-well optical plate at longitudinal orientation. OPTI-MEM medium with 2.5%FBS was added in the presence of various combinations of soluble factors (rhVEGF 30ng/ml,

S1P 1µM, Peprotech and Cayman Chemical) or mouse BM cells previously transduced with LVs (BM_hVEGF, BM_SPHK1). Ten rings per group were kept in the culture for 7 days and the medium was changed at day 4 and 6. Rings were rinsed with a PBS with ions and fixed with 1.6% PFA for 30min, RT. Afterwards, permeabilization with PBLEC solution (PBS with ions, 0.1mM $MnCl_2$, 1% Tween-20) in two 15min incubations at RT was performed, followed by blocking with DACO buffer (protein block serum free #X0909) 30min at 37°C. Primary reagents Isolectin B4 (IB4, in the case of experiments with soluble cytokines) or anti-CD31 (in experiments using bone marrow, BM, cells) at concentration 1:150 and anti-SMA-Cy3 (1:400) in 50µl of PBLEC buffer per well were incubated overnight at 4°C. After washing with PBS 0.1% Triton X-100, incubation with secondary antibodies: streptavidin-488 (1:200) or anti-hamster-647 (1:500) and Hoechst (1:10 000) was performed for 3h at RT. Rings were washed and embedded by adding 1 drop of Fluoromont to each well and kept in 4°C protected from light. Imaging was performed using Nikon A1R confocal system coupled to a Nikon Ti-Eclipse microscope using 10x objective and capturing 400µm in depth with z-stack every 3µm. Analysis of images was performed using a Matlab-based method for 3D-microvasculature developed in our lab, and using Imaris software. Antibodies used are summarized in Table 4.

In vivo mouse experiment protocol

Three days after I/R surgery, echocardiography was performed to confirm myocardial infarction. Four days post I/R, mice were intravenously injected with $5x10^6$ BM cells transduced with LV_hVEGF in 100µl of PBS or with PBS as a control group. 24h after first injection, blood samples were collected via facial vein into EDTA coated tubes. Seven days post I/R, a second injection was performed, with $5x10^6$ BM cells transduced with LV_hSPHK1 and blood was collected 24h after injection. At day 28, endpoint echography was performed and mice were sacrificed using a CO_2 chamber. Blood samples were collected and hearts, lungs and livers were weighed and collected. Heart perfusion was performed through aorta using 5-10ml of cold PBS. Organs were immediately put in 0.4% PFA for overnight incubation at 4°C. After washing with PBS, samples were incubated in 20% and 40% sucrose until they sank. For long-term storage, organs were embedded in OCT and kept in -80°C. For plasma collection, harvested blood

samples were centrifuged at 2000g for 10min, followed by supernatant centrifugation at 2500g for 15min. Next, samples were snap frozen in liquid nitrogen and kept at -80ºC for S1P and hVEGFA detection.

Cardiac ischemia/reperfusion in mice

10-12 week old mice were pre oxygenated with 100% O_2 for 5 min and anaesthetized with a combination of 10mg/kg Alfaxalone (Alfaxan®), 1mg/kg Medetomidine (Medeson®) and 2mg/kg Midazolam (Dormicun®). Mouse body temperature was maintained using a warmed 38ºC pad, and they were ventilated with 100% O_2 (120 breaths per minutes 8ml/kg of tidal volume) using Minivent 680 ventilator (Harvard apparatus). Without damaging left pectoral muscles, thoracic space was exposed between the 4th and 5th ribs. After a soft pericardiectomy, the left anterior descendent (LAD) coronary artery was visualized and occluded with a small piece of P10 fixed laterally with 7/0 nylon suture (Prolene®). LAD coronary artery reperfusion was allowed after 45 minutes, just releasing the suture and tubing pressure over the vessel. Reperfusion was confirmed after visualization of reddish heart color. For recovery, 2mg/kg of atipamezol (Revertor®) was inoculated IP and mice were extubated once they become conscious. To keep post-surgery analgesia, we inoculated SC with 0.1mg/kg of buprenorphine (Buprex®) and 320mg/kg of Paracetamol in drinking water for 3 days.

Echocardiography

Echocardiography was performed by an operator blinded to the study using a high-frequency ultrasound system (Vevo 2100, Visualsonics Inc., Canada) with a 30-MHz linear probe. Mice were lightly anesthetized with 0.5-2% isoflurane in oxygen, administrated through a nose cone. Echocardiography was acquired in supine position using a heating platform and warmed ultrasound gel to maintain body temperature. Standard two-dimensional echocardiography (2D) and M-mode was performed in parasternal long axis view and parasternal short axis view. Images were acquired and analyzed later by a blinded expert using Vevo 2100 software. Cardiac parameters such as end-diastolic and end-systolic volumes, stroke volume and left ventricular ejection fraction were quantified using area length.

LV transduction and flow cytometry analysis of mouse BM cells

Mouse BM cells were harvested from 9-12 weeks old BL6 mice by flushing femurs and tibias with cold PBS with the addition of 2% FBS. Red blood cell depletion was performed by adding sterile H_2O miliQ on the cell pellet followed immediately with the addition of a large volume of PBS 2% FBS. Cells were cultured on non-adherent plates in 199 medium (Lonza), 10% FBS, 100U/ml penicillin, 100U/ml streptomycin in presence of murine cytokines: 20ng/ml M-CSF and 100ng/ml SCF (Peprotech). After overnight incubation, cells were counted using trypan blue and resuspended at $2x10^6$ cells/ml. Transduction was performed by adding LVs at multiplicity of infection (MOI 50) and incubated overnight in a 6-well non-adherent plate. Subsequently, cells were harvested and washed by adding a large amount of PBS 2% FBS to remove virus particles. After centrifugation, cells were resuspended in PBS 2% FBS, counted, washed again in ~40ml of PBS, and filtered through a 70µm cell mesh. For intravenous injection, cell pellet was resuspended in PBS at concentration 100µl per $5x10^6$ cells. To analyze BM cell subsets, the flow cytometry technique was used. After washing the virus blocking with 100µl of 1:100 Fc block (Mouse BD Fc Block, Purified Rat Anti-Mouse CD16/CD32) in FACS buffer (2.5% FBS, 0.5mM EDTA in PBS) was performed for 20min at 4°C. Next, cells were washed with 2ml of FACS buffer and centrifuged. Subsequently, cells were stained with $1ul/10^6$ cells CD11b-Alexa fluor-647, $2µl/1x10^6$ cells F4/80-PE-Cy7, $1.5µl/1x10^6$ cells Ly6C-FITC, $2µl/1x10^6$ cells CCR2-PE and $2µl/1x10^6$ cells CX_3CR1-Pacific Blue (Table 3) in 100µl of FACS buffer for 15min in RT protected from light. After washing cells were resuspended in 150µl of FACS buffer with addition of 5µl live/death dye 7-AAD (BD Pharmingen) per sample. Sample acquisition was performed using BD LSRFortessa.

Table 3. List of antibodies used for FACS staining

Name	**Clone, company**
CD11b-Alexa fluor-647	M1/70, BD
F4/80-PE-Cy7	BM8, Biolegend
Ly6C-FITC	AL-21, BD Pharmingen
CCR2-PE	475301, R&D

CX3CR1-Pacific Blue SA011F11, Biolegend

Immunohistochemistry and immunofluorescence analysis

Sections of 15µm were cut and washed in PBS for 5 min, and permeabilized for 10min in 0.1% Triton in PBS at RT. Blocking in 10% BSA, 0.1% Triton in PBS was performed for 1h in a wet chamber at RT. Primary antibodies were incubated in blocking buffer overnight in a wet chamber at 4°C. After washing with 0.1 Triton PBS, slides were incubated with primary antibodies for 1.5h in a wet chamber protected from light at RT. Subsequently, slides were washed twice in 0.1% Triton PBS and once in PBS for 10min and mounted with Fluoromont G (Southern Biotech). For microvasculature staining, the primary antibodies hamster anti-CD31 (1:150), rat anti-PDGFRβ (1:150) and α-SMA-Cy3 (1:400); the secondary antibodies goat anti-hamster Alexa Fluor-647, chicken anti-rat Alexa Fluor-488 (1:500), and Hoechst (1:10.000) were used. Images were acquired with a Leica SP5 confocal microscope using 40x objective (NA 1.25) with oil immersion. Z-stacks were acquired every 1µm. To quantify cardiomyocyte size and macrophage content, the primary antibody rabbit anti-Laminin (1:50), the secondary antibody chicken anti-rabbit-488 (1:500), and Hoechst (1:10.000) were used. Fibrosis was assessed based on Masson-Trichrome staining and tissue was visualized using NanoZoomer-2.ORS® (Hamamatsu). In the homing experiment, tissue slices were stained with anti-RFP-594 antibody and Hoechst with 1:300 and 1:10 000 dilutions respectively. Sections from OCT-included tissue were permeabilized and blocked in PBS containing 0.3% Tx100, 5% BSA, 5% goat serum for 1h at RT. Samples were then incubated overnight at 4°C with anti-α-actinin, anti-Atp2a2, or anti-cleaved caspase-3 at 1:100 dilution and with the corresponding secondary antibodies and Hoechst 33342 for 2h at RT. Samples were finally mounted in Fluoromount-G, and images acquired with a Nikon A1R confocal microscope fitted with a 20x objective and processed using Image J software.

Table 4. List of antibodies /reagents used for immunostaining

Name	**Species**	**Clone, company**
α-actinin	rabbit	Thermo Fisher (PA5-21396)

anti-goat-568	donkey	Molecular Probes (A-11057)
anti-hamster-647	goat	Jackson ImmunoResearch (127-605-160)
anti-mouse-647	chicken	Molecular Probes (A-21463)
anti-rabbit-488	chicken	Molecular Probes (A-21441)
anti-rat-488	chicken	Molecular Probes (A-21472)
anti-rat-568	goat	Molecular Probes (A-11077)
anti-RFP-594	rabbit	polyclonal, Biotium (#20422)
Atp2a2	mouse	Novusbio (NB100-237)
CD31	hamster	2H8, Merck
CD68	rat	FA-11, Serotec
Cleaved caspase-3	rabbit	Cell Signaling (9661S)
Hoechst 33342	-	Invitrogen (H1399)
IB4-biotynylated	-	Vector Laboratories (B-1205)
Laminin	rabbit	Sigma (L9393)
PDGFRβ	rat	APB5, eBioscience
SMA unconjugated	mouse	1A4, Sigma
SMA-Cy3	mouse	1A4, Sigma
streptavidin-488	-	Invitrogen (S32354)

Image analysis

Analysis of heart roundness was performed on images of the hearts after dissection using ImageJ software[4]. Roundness was calculated as $4 \cdot \frac{area}{\pi \cdot major\ axis^2}$. To quantify cardiomyocyte size, ImageJ based semi-automated macro was designed. Cardiomyocytes recognized by surrounding laminin staining were quantified by area and perimeter. Subsequently, all images were revised by eye and incorrectly recognized ones were removed and/or labelled manually. Quantification of fibrosis was performed using ImageJ software on seven sequential 15µm-thick cuts from the apex to the base of the heart. Results are represented as a percentage of fibrotic tissue area to the left ventricle area.

For the analysis of the coronary microvasculature 2 to 3 transverse 15 μm-thick slices were stained from each heart and two confocal microscopy images were obtained from each slice in the infarct and the remote zones (sections acquired every 1 μm) with a total of 192 3D images quantitated. Acquisition of the images was standardized to capture similar infarcted (in the anterior left ventricle free wall) and remote (in the spare left ventricle wall most distant to the infarct) zones in the different hearts. The analysis was based on a fully automatic 3D image analysis pipeline developed at our laboratory to perform in-depth analysis of microvascular data. The pipeline, which consists of several modules, has been described in detail in[5] and it permits the calculation of a pool of parameters that quantify all major features of the microvasculature. In this work, modifications and an additional module have been incorporated into the pipeline to account for the different behavior of the staining markers between mouse and porcine tissue, and for the particular nature of the mouse microvasculature.

The majority of images of all channels (Hoechst, CD31, SMA, PDGFRβ) were segmented using the MMT algorithm as in the original pipeline[5]. However, there was a subset of images of the SMA^+ channel, which were segmented using an ad-hoc ImageJ plugin, since they presented additional artifacts introduced during the acquisition process and they required specific treatment. We classify the vessels in: (i) capillaries $CD31^+$ and SMA^- vessels of diameter < 5μm; (ii) enlarged capillaries, $CD31^+$ and SMA^- vessels of diameter $\geq$5μm; and (iii) SMA+ vessels (mostly corresponding to arterioles), $CD31^+$ and SMA^+ vessels of diameter > 5μm. The reason for this categorization is two-fold; first in the case of the mouse microvasculature, the particular anti-α-SMA antibody we used did not stain the venules; second, based, on previously made measurements in various species and tissues[6-9], we consider as capillaries vessels of diameter < 5 microns. Towards classifying the vascular volume in the above three categories, 3D Frangi filtering was applied on the CD31 segmentation in order to create a volume than contains the microvessels with diameters larger than 5 microns. The calculated volume was afterwards used in conjunction with the segmentation of SMA^+ and CD31 channels, to categorize voxels of the CD31 segmentation into one of the three categories. It is worth noting that the segmentation of SMA^+ had been previously expanded by 3 microns to better overlap with the CD31 staining. This process resulted in three

new image volumes, each of which contained vessels of only one category. Based on the Minkowski functionals, we calculated the volume and surface density for the different classes of the vasculature, along with the percentage that the volume of each class represented over the overall vascular volume. We also estimated the oxygen diffusion efficiency based on our calculation of 3D extravascular distances (distance of every point to the closest vessel)[5] as previously reported[10].

We have also added a module in order to quantify the information regarding PDGFRβ$^+$ cells in the tissue. More precisely, we calculated the percentage of vessels covered with PDGFRβ, as well as an indicator of myofibroblast abundance similar to the damage index of the original approach[5]. For the latter, based on the calculated SMA$^+$ thickness, we assumed that the maximum coverage of a vessel with PDGFRβ would be 10 microns. We therefore dilated the segmentation of the CD31 channel by 10 microns so that the covered vessels would overlap with their coverage of PDGFRβ. Subsequently, the non-overlapping parts of the PDGFRβ cells were considered as myofibroblasts. Lastly, the myofibroblasts abundance was calculated as the ratio of the volume of the overlapping PDGFRβ$^+$ voxels over the complete volume of PDGFRβ$^+$ voxels.

Western blot

Protein was extracted from OCT-embedded mouse heart sections (9 to 15 sections of 3μm each) by direct incubation in lysis buffer (2%SDS and 20mM Tris-HCl pH 7.5 supplemented with protease and phosphatase inhibitors). Proteins were resolved by 8% (non-reducing) or 10% (reducing) SDS-PAGE (for Col1a1 and Atp2a2 respectively). Proteins were transferred to nitrocellulose membranes, blocked in 5% BSA, and incubated sequentially with primary and horseradish peroxidase (HRP)-conjugated secondary antibodies. We used primary antibodies against Col1a1 (Santa Cruz Biotechnology, SC-293182), Atp2a2 (Novusbio, NB100-237), tubulin (Sigma, T6074), and GAPDH (Sigma, G9545); all at 1:1000 dilution. The secondary antibodies were HRP-goat anti-mouse and HRP-goat anti-rabbit (Jackson), which were visualized with Luminata Classico Western HRP Substrate (Millipore, WBLUC0500) in ImageQuant Las4000 (GE Healthcare Life Sciences, Massachusetts, USA). Western blots were quantified using Image J software (https://imagej.nih.gov/ij/).

References

1. Squadrito ML, Pucci F, Magri L, Moi D, Gilfillan GD, Ranghetti A, Casazza A, Mazzone M, Lyle R, Naldini L and De Palma M. miR-511-3p modulates genetic programs of tumor-associated macrophages. Cell Rep. 2012;1:141-54.
2. Dai L, Qi Y, Chen J, Kaczorowski D, Di W, Wang W and Xia P. Sphingosine kinase (SphK) 1 and SphK2 play equivalent roles in mediating insulin's mitogenic action. Mol Endocrinol. 2014;28:197-207.
3. Baker M, Robinson SD, Lechertier T, Barber PR, Tavora B, D'Amico G, Jones DT, Vojnovic B and Hodivala-Dilke K. Use of the mouse aortic ring assay to study angiogenesis. Nat Protoc. 2011;7:89-104.
4. Schindelin J, Arganda-Carreras I, Frise E, Kaynig V, Longair M, Pietzsch T, Preibisch S, Rueden C, Saalfeld S, Schmid B, Tinevez JY, White DJ, Hartenstein V, Eliceiri K, Tomancak P and Cardona A. Fiji: an open-source platform for biological-image analysis. Nat Methods. 2012;9:676-82.
5. Gkontra P, Norton KA, Zak MM, Clemente C, Aguero J, Ibanez B, Santos A, Popel AS and Arroyo AG. Deciphering microvascular changes after myocardial infarction through 3D fully automated image analysis. Sci Rep. 2018;8:1854.
6. Kassab GS and Fung YC. Topology and dimensions of pig coronary capillary network. Am J Physiol. 1994;267:H319-25.
7. Kayar SR, Hoppeler H, Armstrong RB, Laughlin MH, Lindstedt SL, Jones JH, Conley KR and Taylor CR. Estimating transit time for capillary blood in selected muscles of exercising animals. Pflugers Arch. 1992;421:578-84.
8. Mayrovitz HN. Skin capillary metrics and hemodynamics in the hairless mouse. Microvasc Res. 1992;43:46-59.
9. Asaishi K, Endrich B, Gotz A and Messmer K. Quantitative analysis of microvascular structure and function in the amelanotic melanoma A-Mel-3. Cancer Res. 1981;41:1898-904.
10. Cassot F, Lauwers F, Fouard C, Prohaska S and Lauwers-Cances V. A novel three-dimensional computer-assisted method for a quantitative study of microvascular networks of the human cerebral cortex. Microcirculation. 2006;13:1-18.